

THE MID-INFRARED HIGH-IONIZATION LINES FROM ACTIVE GALACTIC NUCLEI AND STAR FORMING GALAXIES*

MIGUEL PEREIRA-SANTAELLA^{1,2}, ALEKSANDAR M. DIAMOND-STANIC³, ALMUDENA ALONSO-HERRERO^{1,2,4}, AND GEORGE H. RIEKE³

Accepted for publication in ApJ on 10 October 2010

ABSTRACT

We used *Spitzer*/IRS spectroscopic data on 426 galaxies including quasars, Seyferts, LINER and H II galaxies to investigate the relationship among the mid-IR emission lines. There is a tight linear correlation between the [Ne V]14.3 μm and 24.3 μm (97.1 eV) and the [O IV]25.9 μm (54.9 eV) high-ionization emission lines. The correlation also holds for these high-ionization emission lines and the [Ne III]15.56 μm (41 eV) emission line, although only for active galaxies. We used these correlations to calculate the [Ne III] excess due to star formation in Seyfert galaxies. We also estimated the [O IV] luminosity due to star formation in active galaxies and determined that it dominates the [O IV] emission only if the contribution of the active nucleus to the total luminosity is below 5%. We find that the AGN dominates the [O IV] emission in most Seyfert galaxies, whereas star-formation adequately explains the observed [O IV] emission in optically classified H II galaxies. Finally we computed photoionization models to determine the physical conditions of the narrow line region where these high-ionization lines originate. The estimated ionization parameter range is $-2.8 < \log U < -2.5$ and the total hydrogen column density range is $20 < \log n_{\text{H}} (\text{cm}^{-2}) < 21$.

Subject headings: galaxies: active — galaxies: nuclei — galaxies: starburst — infrared: galaxies

1. INTRODUCTION

Primarily through measurements in the optical, active galactic nuclei (AGNs) have been categorized as Type 1 or 2, respectively with and without very broad emission lines. The unification model (Antonucci 1993; Urry & Padovani 1995) successfully explains this behavior in terms of a dusty circumnuclear torus that hides the broad-line region (BLR) from our line of sight for type 2 AGN. It also appears that extinction in the host galaxy can hide the BLR (e.g., Maiolino & Rieke 1995; Alonso-Herrero et al. 2003) in some active galaxies. Extinction therefore affects the optical properties of AGN in fundamental ways. These effects can be minimized by studying these objects using infrared (IR) emission lines, both to test the predictions of the unification model and to characterize AGNs in a uniform way. Toward this end, we have used mid-IR observations with the Infrared Spectrograph (IRS, Houck et al. 2004) on *Spitzer* to examine the behavior of a large sample of AGN.

Important high-ionization lines accessible in the mid-IR include [Ne V] (97.1 eV) at 14.32 and 24.32 μm , [O IV] (54.9 eV) at 25.89 μm , and [Ne III] (41 eV) at 15.56 μm . Because of their very high ionization potential, the [Ne V] lines are considered to be reliable

pereira@damir.iem.csic.es

* This work is based on observations made with the Spitzer Space Telescope, which is operated by the Jet Propulsion Laboratory, California Institute of Technology under NASA contract 1407

¹ Instituto de Estructura de la Materia, CSIC, Serrano 121, E-28006, Madrid, Spain

² Departamento de Astrofísica, Centro de Astrobiología, CSIC/INTA, Carretera de Torrejón a Ajalvir, km 4, 28850, Torrejón de Ardoz, Madrid, Spain

³ Steward Observatory, University of Arizona, 933 North Cherry Avenue, Tucson, AZ 85721, USA

⁴ Associate Astronomer, Steward Observatory, University of Arizona, AZ 85721, USA

signposts for an AGN (Genzel et al. 1998; Armus et al. 2007). These lines have been used to estimate the accretion power in the local Universe (Tommasin et al. 2010) and to identify low-luminosity AGNs in local galaxies (Satyapal et al. 2008; Goulding & Alexander 2009). However, they are also produced in supernova remnants (SNR, Oliva et al. 1999; Smith et al. 2009), planetary nebulae (PN, Pottasch et al. 2009), and Wolf-Rayet stars (WR, Schaerer & Stasińska 1999). Although the [Ne V] luminosities of these objects are low, $\sim 10^{34} \text{ erg s}^{-1}$ (Smith et al. 2009; Pottasch et al. 2009), several thousands of them might also produce detectable [Ne V] emission.

Despite the lower ionization potential of [O IV], the 25.89 μm emission line appears to be an accurate indicator of AGN power, since it correlates well with the hard ($> 14 \text{ keV}$) X-ray luminosity (Meléndez et al. 2008a; Rigby et al. 2009; Diamond-Stanic et al. 2009) and the mid-IR [Ne V] emission lines (Dudik et al. 2009; Weaver et al. 2010). However, this line also appears in the spectra of starburst galaxies with no other evidence for AGN (Lutz et al. 1998a; Bernard-Salas et al. 2009), where it is attributed to Wolf-Rayet stars (Crowther et al. 1999; Schaerer & Stasińska 1999) and/or to shocks (Allen et al. 2008; Lutz et al. 1998a).

The [Ne III] 15.56 μm line is excited by young, massive stars (Verma et al. 2003; Brandl et al. 2006; Beirão et al. 2006, 2008; Ho & Keto 2007; Bernard-Salas et al. 2009; Alonso-Herrero et al. 2009; Pereira-Santaella et al. 2010). Nonetheless, it seems to be a reasonably good proxy for AGN luminosity, at least for reasonably high luminosities (Gorjian et al. 2007; Dudik et al. 2009; Meléndez et al. 2008a; Tommasin et al. 2008). Quantifying when its excitation is dominated by an active nucleus would allow it to be used in concert with the other high-

ionization lines to probe conditions in the neighborhoods of AGNs.

In this paper, we present a statistical study of the behavior of these lines in a sample of 426 galaxies. The data are compiled from the literature on high spectral resolution ($R \sim 600$) IRS measurements, as well as our own new measurements of low-luminosity Seyfert galaxies and luminous infrared galaxies (LIRGs). We describe the sample and the data reduction respectively in Sections 2 and 3. Section 4 explores the correlations among the high-ionization emission lines. In Section 5, we discuss the star formation contribution to these lines. Section 6 compares the star formation in Seyfert 1 and 2 galaxies. Finally, in Section 7 we use photoionization models to study the physical conditions in the narrow line regions (NLRs).

Throughout this paper we assume a flat cosmology with $H_0 = 70 \text{ km s}^{-1}\text{Mpc}^{-1}$, $\Omega_M = 0.3$, and $\Omega_\Lambda = 0.7$.

2. THE SAMPLE

The sample contains 426 galaxies (Table 1) for which high spectral resolution ($R \sim 600$) *Spitzer*/IRS spectra were available, either in the literature (Weedman et al. 2005; Ogle et al. 2006; Farrah et al. 2007; Gorjian et al. 2007; Tommasin et al. 2008, 2010; Veilleux et al. 2009; Dale et al. 2009; Bernard-Salas et al. 2009; Goulding & Alexander 2009; Pereira-Santaella et al. 2011, in prep.), in the *Spitzer* archive or observed through the programs 40936 and 50597 (PI: G. H. Rieke). AGN type classifications were taken from NASA Extragalactic Database (NED). We designated only pure cases as Type 2 and included within Type 1 all intermediate cases (i.e.: 1.2, 1.5, 1.8, 1.9) based on observations and modeling of the nuclear spectra energy distributions (Alonso-Herrero et al. 2003; Ramos Almeida et al. 2009). We could not find the nuclear activity classification for 32 of the galaxies. The sample includes 28 QSOs, 76 Seyfert 1, 125 Seyfert 2, 55 LINERs and 110 H II or starburst galaxies (see Table 2). The luminosity of the active galaxies ranges from QSO (QUEST sample, Veilleux et al. 2009) to typical Seyfert galaxies ($12 \mu\text{m}$ sample, Rush et al. 1993; Tommasin et al. 2010), relatively low-luminosity Seyferts (RSA sample, Maiolino & Rieke 1995; Ho et al. 1997; Diamond-Stanic et al. 2009) and LINERs (Sturm et al. 2006). According to their infrared luminosities 71 sample members are classified as LIRGs ($L_{\text{IR}} = 10^{11} - 10^{12} L_\odot$) and 54 as ultraluminous infrared galaxies (ULIRGs, $L_{\text{IR}} > 10^{12} L_\odot$). We found in the Revised Bright Galaxy Sample catalog (Sanders et al. 2003; Surace et al. 2004) the *IRAS* fluxes for 196 of our galaxies which we used to calculate their L_{IR} as defined in Sanders & Mirabel (1996).

Note that the LINER group includes very different galaxies. IR-bright LINERs ($L_{\text{IR}}/L_B \gtrsim 1$) have infrared SEDs similar to starbursts, although high-ionization lines and hard X-ray cores are detected in some, suggesting the presence of an AGN. In comparison, IR-faint LINERs ($L_{\text{IR}}/L_B \lesssim 1$) seem to be powered by an AGN (Sturm et al. 2006; Satyapal et al. 2004).

Figure 1 shows the distance distribution of the sample. The median distance is 60 Mpc and most (68%) of the galaxies are between 15 and 400 Mpc.

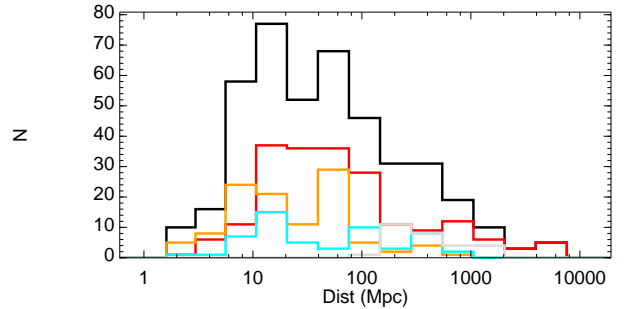


FIG. 1.— Distribution of the galaxy distances of the complete sample (black), QSO (gray), Seyfert 1 and 2 galaxies (red), LINERs (blue) and H II galaxies (orange).

TABLE 2
THE SAMPLE

Type	N	[Ne V]14.3 μm	[Ne V]24.3 μm	[O IV]
QSO	28	22	16	25
Seyfert 1	76	59	42	63
Seyfert 2	125	89	69	101
LINER	55	10	6	27
H II/Starburst	110	4	2	59
Unknown	32	2	1	7
Total	426	186	136	282

NOTE. — N is the number of galaxies of each type. For each type we give the number of detections of the [Ne V]14.32 μm , [Ne V]24.32 μm and [O IV]25.89 μm emission lines.

3. DATA REDUCTION

In addition to results from the literature, we utilized the measurements for the 88 galaxies of the RSA sample observed with the high spectral resolution modules as well as for the 34 LIRGs of the Alonso-Herrero et al. (2006) sample (3 of these LIRGs are also members of the RSA sample). We retrieved the basic calibrated data (BCD) from the *Spitzer* archive processed by the pipeline version S18.7. We subtracted the background contribution when a dedicated sky observation was available. Note however that the sky subtraction is not important to measure these fine structure emission lines and it just improves the final quality of the spectra by removing bad pixels. Then we extracted the spectra using the standard programs included in the *Spitzer* IRS Custom Extraction (SPICE) package provided by the *Spitzer* Science Center (SSC). We assumed the point source calibration for all the galaxies, which is a good approximation for most of the galaxies at least for the high ionization lines. For the galaxies observed in the mapping mode we extracted the nuclear spectra from the data cubes using a square aperture of $13''.4 \times 13''.4$ and then we applied an aperture correction (Pereira-Santaella et al. 2011, in prep.). We used a Gaussian profile to fit the emission lines. For 9 galaxies (NGC 777, NGC 3254, NGC 3486, NGC 3941, NGC 4138, NGC 4378, NGC 4472, NGC 4698, NGC 5631) we were not able to measure any spectral feature due to the low signal-to-noise ratio of the spectra. They are not listed in Table 1 nor included in the analyzed sample.

Table 2 includes the number of detections of the [Ne V]14.32 μm , [Ne V]24.32 μm and [O IV]25.89 μm

TABLE 3
MEDIAN LINE RATIOS

Ratio	Median ratio				
	QSO	Sy1	Sy2	LINER	H II
[O IV]25.89 μm /[Ne V]24.32 μm	3.3 \pm 1.2*	3.6 \pm 0.6	3.5 \pm 0.6	3.7 \pm 1.0*	4.1 \pm 1.3*
[O IV]25.89 μm /[Ne V]14.32 μm	3.6 \pm 0.9	3.5 \pm 1.0	3.5 \pm 1.3	4.8 \pm 2.0*	4.4 \pm 2.0*
[Ne V]24.32 μm /[Ne V]14.32 μm	1.0 \pm 0.3*	1.1 \pm 0.3	1.0 \pm 0.3	1.3 \pm 0.3*	4.7 \pm 4.1*
[Ne III]15.56 μm /[Ne V]14.32 μm	1.7 \pm 0.5	1.9 \pm 0.6	2.0 \pm 0.7	5.3 \pm 3.7*	6.8 \pm 1.7*
[Ne II]12.81 μm /[Ne V]14.32 μm	0.7 \pm 0.4	1.6 \pm 0.7	2.0 \pm 1.1	28 \pm 14*	57 \pm 42*
[Ne III]15.56 μm /[O IV]25.89 μm	0.5 \pm 0.2	0.6 \pm 0.2	0.9 \pm 0.4	2.3 \pm 1.1	4.2 \pm 2.4
[Ne II]12.81 μm /[O IV]25.89 μm	0.2 \pm 0.1	0.5 \pm 0.3	1.1 \pm 0.9	6 \pm 2	22 \pm 16
[Ne III]15.56 μm /[Ne II]12.81 μm	2.0 \pm 1.0	1.2 \pm 0.6	0.8 \pm 0.4	0.3 \pm 0.2	0.17 \pm 0.07

NOTE. — Median ratios and uncertainties for each type of galaxies. The uncertainty is calculated as the median absolute deviation (should be multiplied by 1.48 to obtain the standard deviation).

* These values are calculated with less than 20 galaxies.

emission lines and in Table 3 we show the observed median line ratios for each galaxy type both for galaxies from literature and those analyzed by us. Note that there are 4 detections of the [Ne V]14.32 μm line and 2 of the [Ne V]24.32 μm line in galaxies classified as H II. For these galaxies (NGC 613, NGC 1792, NGC 3621 and NGC 5734) the detection of the [Ne V] lines is the only evidence of AGN activity. We decided to keep their H II classification because: (1) the AGN may be extremely obscured or very low luminosity and, thus, the nuclear spectra might be dominated by star formation features; and (2) these lines are also detected in SNR, PN and WR stars which could be the origin of the [Ne V] emission in these galaxies.

Table 3 gives the median and deviation of all the line ratios we discuss in this paper for each type of galaxy. The line fluxes for all the galaxies are listed in Table 1.

4. THE MID-IR HIGH-IONIZATION EMISSION LINES

4.1. The [O IV] versus [Ne V] correlations

The [Ne V]24.32 μm and the [O IV]25.89 μm emission lines are commonly detected in active galaxies (Lutz et al. 1998b; Genzel et al. 1998; Tommasin et al. 2010). The detection of the former is considered a good indicator of AGN activity because of its high ionization potential. However using the [O IV]25.89 μm line as an AGN tracer is not as straightforward. For optically classified Seyfert galaxies the [O IV]25.89 μm luminosity is a good proxy for the AGN intrinsic luminosity (Diamond-Stanic et al. 2009; Meléndez et al. 2008a) and there is a good correlation between the [Ne V]24.32 μm and the [O IV]25.89 μm emission in AGNs (Dudik et al. 2009; Weaver et al. 2010). However, the [O IV]25.89 μm line is also produced by WR stars (Schaerer & Stasińska 1999) and is observed in starburst galaxies with no other evidence for the presence of an AGN (Lutz et al. 1998a; Bernard-Salas et al. 2009).

The left panel of Figure 2 shows the tight correlation between the [Ne V]24.32 μm and [O IV]25.89 μm lines spanning at least 5 orders of magnitude in luminosity ($38 < \log L_{[\text{O IV}]} (\text{erg s}^{-1}) < 43$). We do not find any dependence between the optical classification of the nuclear activity and this correlation. This implies that the ionization parameter is similar in type 1 and type 2 Seyfert

galaxies (see Section 7). The slope of the best fit to the luminosity data is 0.96 ± 0.02 with a 0.14 dex dispersion. It is reasonable to assume a linear correlation between these two emission lines, and this yields a ratio [O IV]25.89 μm /[Ne V]24.32 μm = 3.5, with rms scatter of 0.8.

The [Ne V]24.32 μm line is detected in \sim 50% of the optically classified Seyfert galaxies (see Table 2). However, for a considerable number of galaxies we have the [O IV]25.89 μm measurement and an upper limit for the [Ne V]24.32 μm flux. We plot these fluxes and upper limits (middle panel of Figure 2) for all the galaxies. The upper limits to the [Ne V]24.32 μm flux are compatible with the correlation for most of the Seyfert galaxies. However, the [O IV]25.89 μm line is detected in more than 50% of the H II galaxies in our sample. In 90% of these galaxies, the sensitivity of the [Ne V]24.32 μm measurement (or upper limits) is inadequate to probe whether the [O IV] emission is associated with a hidden AGN.

In short, we find that the [O IV]25.89 μm luminosity is well correlated with the intrinsic AGN luminosity (i.e., [Ne V] luminosity) for Seyfert galaxies and quasars with $L_{[\text{O IV}]} > 10^{39} \text{ erg s}^{-1}$ to, at least, $L_{[\text{O IV}]} \sim 10^{43} \text{ erg s}^{-1}$. For lower luminosities the fraction of the [O IV]25.89 μm emission produced by star formation may be considerable. Thus the [O IV]25.89 μm may not be an accurate tracer of the AGN luminosity for galaxies with $L_{[\text{O IV}]} < 10^{39} \text{ erg s}^{-1}$ (Goulding & Alexander 2009).

The linear correlation also holds for the [Ne V]14.32 μm and the [O IV]25.89 μm luminosities (Figure 3), although the dispersion is larger ([O IV]25.89 μm /[Ne V]14.32 μm = 3.4, , with rms scatter of 1.4 assuming a linear fit).

4.2. The [Ne III] and [Ne II] emission lines

Due to the intermediate ionization potential of Ne^{+2} (41.0 eV), the [Ne III]15.56 μm emission line may be produced by young stars or by AGNs. This line is observed in star forming galaxies (Verma et al. 2003; Brandl et al. 2006; Beirão et al. 2006, 2008; Ho & Keto 2007; Bernard-Salas et al. 2009; Dale et al. 2009; Pereira-Santalla et al. 2010), and it is also correlated with the AGN intrinsic luminosity (Gorjian et al. 2007; Deo et al. 2007; Tommasin et al. 2008; Meléndez et al. 2008b).

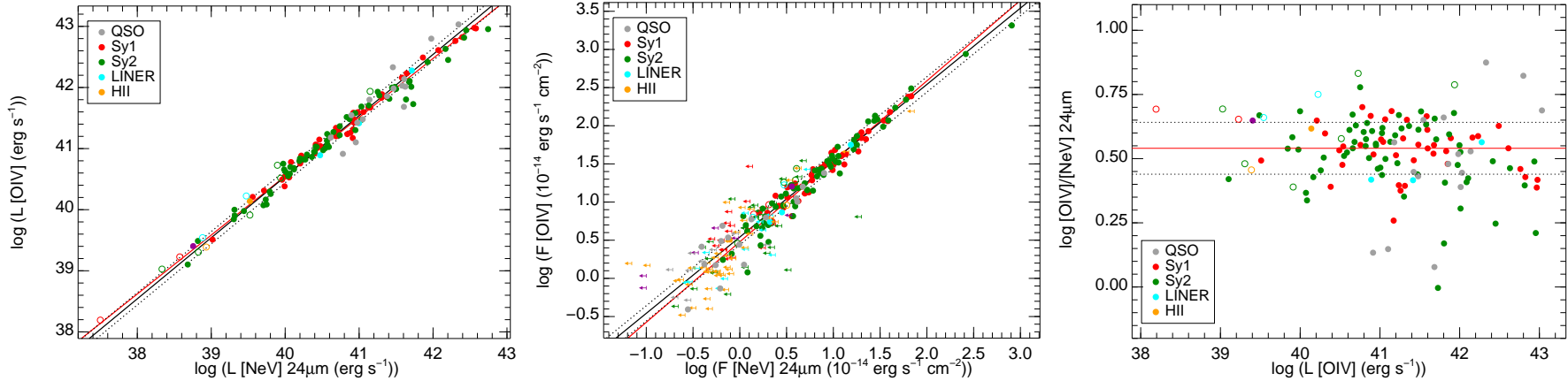


FIG. 2.— Relationship between the [O IV]25.89 μm and [Ne V]24.32 μm luminosities (left) and fluxes (middle). The red line is the best fit and the black line the best linear fit. The dashed lines mark the 1σ deviation. QSO are plotted as gray circles, Sy1 as red circles, Sy2 as green circles, LINERs as blue circles, HII galaxies as orange circles and those galaxies without a classification as purple circles. The open symbols mark the galaxies with star formation which may contribute to the [O IV]25.89 μm emission (see Section 4.2 and right panel of Figure 4). The right panel shows the [O IV]25.89 μm /[Ne V]24.32 μm ratio vs. the [O IV]25.89 μm luminosity. The solid red line is the ratio obtained from the linear fit and the dashed lines mark the 1σ deviation.

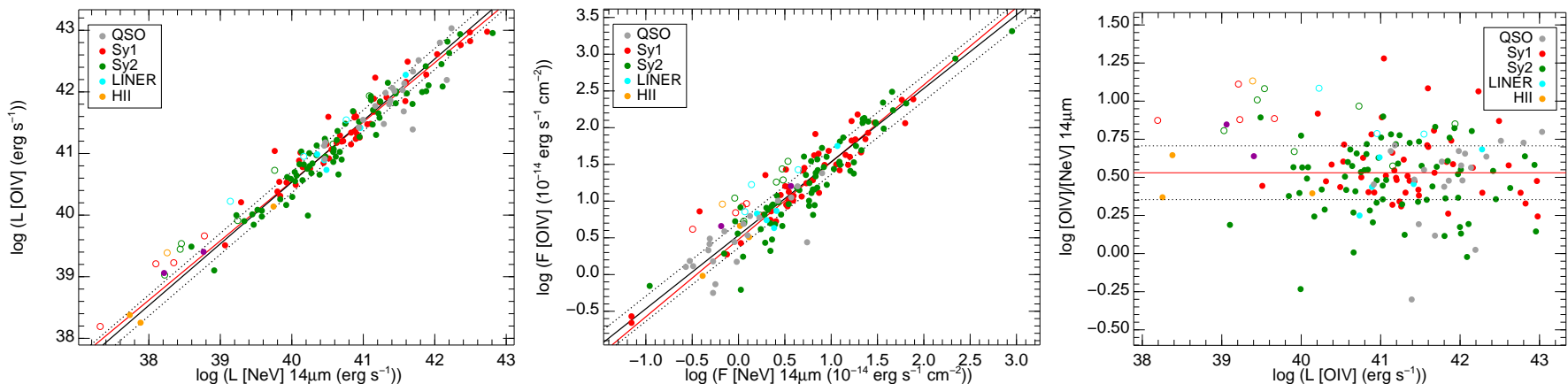


FIG. 3.— Relationship between the [O IV]25.89 μm and [Ne V]14.32 μm luminosities (left) and fluxes (middle). The right panel shows the [O IV]25.89 μm /[Ne V]14.32 μm ratio vs. the [O IV]25.89 μm luminosity. Symbols are as in Figure 2.

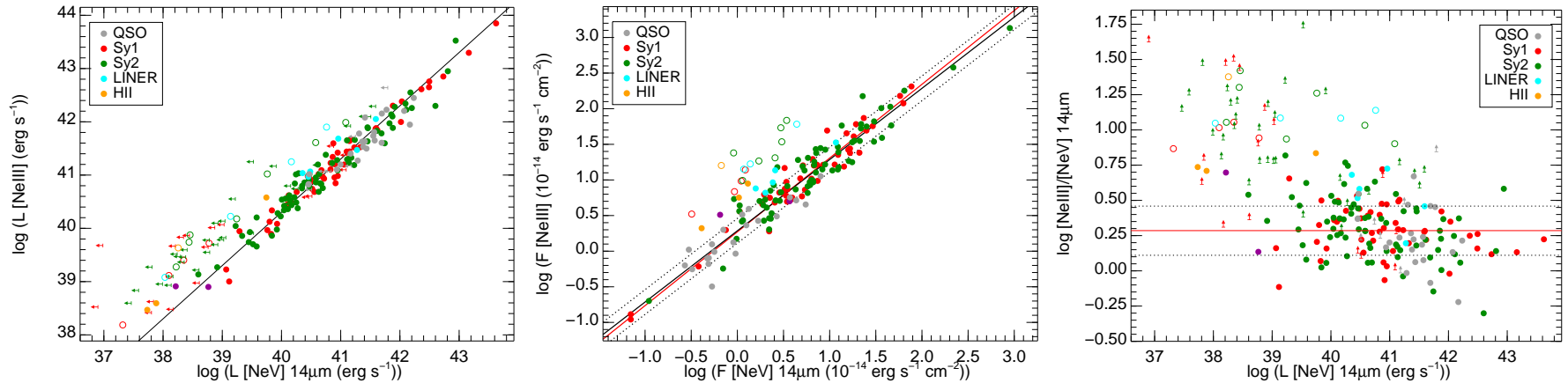


FIG. 4.— Relation between the [Ne III]15.56 μm and [Ne V]14.32 μm emission. Galaxy symbols are as in Figure 2. The open symbols mark those galaxies above 3σ the [Ne V]14.32 μm vs. [Ne III]15.56 μm flux correlation. The black line in the left panel is the ratio obtained from the flux correlation. In the left panel only are included the [Ne V]24.32 μm upper limits of the QSO and Seyfert galaxies.

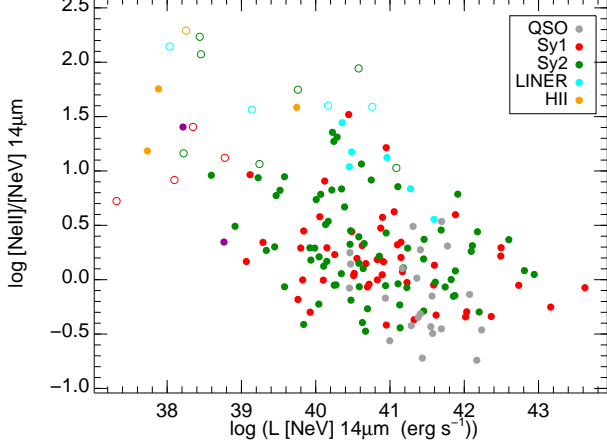


FIG. 5.— $[\text{Ne II}]12.81 \mu\text{m}/[\text{Ne V}]14.32 \mu\text{m}$ ratio vs. $[\text{Ne V}]14.32 \mu\text{m}$ luminosity. Symbols are as in Figure 4.

The middle panel of Figure 4 shows the relation between the observed flux of the $[\text{Ne III}]15.56 \mu\text{m}$ and $[\text{Ne V}]14.32 \mu\text{m}$ emission lines for our sample of AGNs and for the 4 H II galaxies with $[\text{Ne V}]$ detections. We compare these lines because they are close in wavelength and the effect of differential extinction is minimized. It is clear that some galaxies have an excess of $[\text{Ne III}]15.56 \mu\text{m}$ emission relative to that of the $[\text{Ne V}]14.32 \mu\text{m}$, which we attribute to star formation (see Section 5). Therefore to obtain the fit to the data we use the outliers resistant linear fit algorithm provided by the IDL function ROBUST_LINEFIT. The slope of this fit is 1.02 ± 0.02 with a scatter of about 0.2 dex around the fit. The result is consistent with a simple correlation; by fixing the slope to unity, we obtain the ratio $[\text{Ne III}]15.56 \mu\text{m}/[\text{Ne V}]14.32 \mu\text{m} = 1.9$, with rms scatter of 0.8. This correlation was previously reported by Gorjian et al. (2007), although they found a slight dependence of the ratio with the $[\text{Ne V}]14.32 \mu\text{m}$ luminosity (slope 0.89). Their sample included 53 X-ray selected AGNs with $[\text{Ne V}]14.32 \mu\text{m}$ luminosities between 10^{39} and $10^{43} \text{ erg s}^{-1}$. The larger number of galaxies in our sample allows us to minimize the contribution of the galaxies contaminated by star formation to the fit and the luminosity dependence of the correlation is substantially reduced. Where the AGN clearly dominates, the points fall around the line determined for the whole sample by ROBUST_LINEFIT, thus supporting our interpretation that this fit determines the relationship for AGNs in general.

The $[\text{Ne II}]12.81 \mu\text{m}$ emission traces young ($< 10 \text{ Myr}$) star formation (Roche et al. 1991; Thornley et al. 2000; Verma et al. 2003; Rigby & Rieke 2004; Snijders et al. 2007; Ho & Keto 2007; Díaz-Santos et al. 2010). The ionization potential of this emission line is 21 eV and thus it is mainly produced in H II regions. Figure 5 shows that the scatter in the $[\text{Ne II}]12.81 \mu\text{m}/[\text{Ne V}]14.32 \mu\text{m}$ ratio (0.7 dex) is larger than that found in the other line ratios, for the lower AGN luminosities there is a large scatter. There is a weak trend of $[\text{Ne II}]12.81 \mu\text{m}/[\text{Ne V}]14.32 \mu\text{m}$ ratios decreasing with increasing AGN luminosity. Assuming that there is an intrinsic ratio for AGN, this behavior implies that the AGN does not dominate the $[\text{Ne II}]12.81 \mu\text{m}$ output and that there is

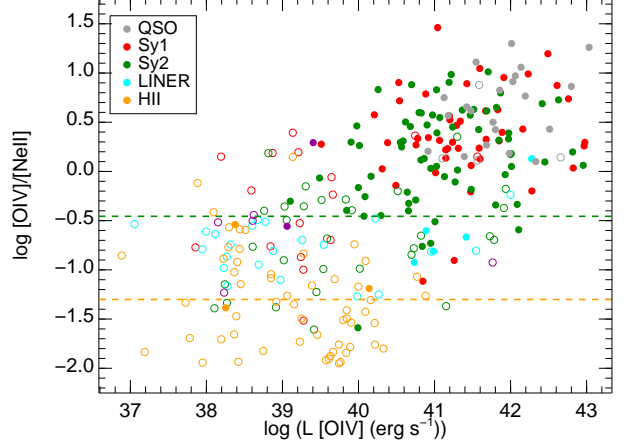


FIG. 6.— $[\text{O IV}]25.89 \mu\text{m}/[\text{Ne II}]12.81 \mu\text{m}$ ratio vs. $[\text{O IV}]25.89 \mu\text{m}$ luminosity. Galaxy symbols are as in Figure 2. The dashed orange ($[\text{O IV}]/[\text{Ne II}] = 0.05$) and green ($[\text{O IV}]/[\text{Ne II}] = 0.35$) lines are the boundaries of the H II and Seyfert galaxies respectively.

a wide range of star formation rates contributing to its luminosity. However, for the most luminous objects ($\log L_{[\text{Ne V}]14\mu\text{m}} (\text{erg s}^{-1}) > 41.5$), the smaller scatter indicates that the relative contribution of the AGN to the total $[\text{Ne II}]12.81 \mu\text{m}$ excitation is higher.

Sturm et al. (2002) determined that the pure AGN $[\text{Ne V}]14.32 \mu\text{m}/[\text{Ne II}]12.81 \mu\text{m}$ ratio is 1.1, but we find many Seyfert galaxies with higher ratios. The largest $[\text{Ne V}]14.32 \mu\text{m}/[\text{Ne II}]12.81 \mu\text{m}$ ratio in our sample is ~ 5.5 , which is compatible with the largest ratio predicted by NLR photoionization models (Groves et al. 2006, their Figure 11). With our data (Figure 5) we are not able to determine the pure AGN ratio, which also depends on the ionization parameter (Groves et al. 2006), but it is likely that it is between that found by Sturm et al. (2002) and the largest ratio in our sample.

The $[\text{O IV}]25.89 \mu\text{m}/[\text{Ne II}]12.81 \mu\text{m}$ ratio can be used to separate AGNs from star-forming galaxies (Genzel et al. 1998; Sturm et al. 2002; Peeters et al. 2004; Dale et al. 2009). We plot this ratio versus the $[\text{O IV}]25.89 \mu\text{m}$ luminosity in Figure 6. Most of the active galaxies have ratios larger than 0.35 whereas the ratios for H II galaxies are lower than 0.05 (Figure 5 of Dale et al. 2009). LINERs appear in the region between these ratios (Figure 6). A considerable number of H II galaxies also have $[\text{O IV}]25.89 \mu\text{m}/[\text{Ne II}]12.81 \mu\text{m}$ ratios above 0.05. The $[\text{Ne V}]$ lines are not detected for them although their upper limits are compatible with the $[\text{O IV}]25.89 \mu\text{m}$ versus $[\text{Ne V}]$ correlations and thus a low-luminosity AGN could be the origin of the $[\text{O IV}]25.89 \mu\text{m}$ emission. The large scatter in the $[\text{O IV}]25.89 \mu\text{m}/[\text{Ne II}]12.81 \mu\text{m}$ ratio, due to the different star formation rates in the AGNs, does not allow us to determine the value of the pure AGN ratio. The largest $[\text{O IV}]25.89 \mu\text{m}/[\text{Ne II}]12.81 \mu\text{m}$ ratios that we find in AGNs are ~ 10 .

5. STAR FORMATION CONTRIBUTIONS TO THE MID-IR HIGH-IONIZATION EMISSION LINES

5.1. $[\text{O IV}]$ Contamination by Star Formation

In Figures 2 and 3 there are few outliers above the $[\text{O IV}]25.89 \mu\text{m}$ versus $[\text{Ne V}]$ correlations. Most of them are represented by open symbols, which indicate that

their $[\text{Ne III}]15.56\mu\text{m}/[\text{Ne V}]14.32\mu\text{m}$ ratios (see Section 5.2) are larger than those found in AGN dominated galaxies (QSO, Sy1 and Sy2). It is likely that the $[\text{O IV}]25.89\mu\text{m}$ emission of these galaxies is contaminated by star formation. We now compare the $[\text{O IV}]25.89\mu\text{m}/[\text{Ne II}]12.81\mu\text{m}$ ratio in star forming regions and AGN. The $[\text{O IV}]25.89\mu\text{m}/[\text{Ne II}]12.81\mu\text{m}$ ratio in star forming regions is < 0.05 (Section 4.2). Taking this upper limit and using the relation between the $[\text{Ne II}]12.81\mu\text{m}$ luminosity and the total infrared ($8\text{-}1000\mu\text{m}$) luminosity (L_{IR}) from Ho & Keto (2007) we obtain the following relation for star-forming galaxies.

$$\log L_{[\text{O IV}]} \text{ (erg s}^{-1}) < \log L_{\text{IR}} \text{ (erg s}^{-1}) - 4.7 \pm 0.6 \quad (1)$$

Rigby et al. (2009) calculated the ratio between the total AGN luminosity and the $[\text{O IV}]25.89\mu\text{m}$ emission. We use the ratio for type 1 AGNs (~ 2500) because the hard X-ray ($E > 10\text{ keV}$) emission used for the bolometric corrections may be affected by extinction in Seyfert 2s (Rigby et al. 2009).

$$\log L_{[\text{O IV}]} \text{ (erg s}^{-1}) = \log L_{\text{AGN}} \text{ (erg s}^{-1}) - 3.4 \pm 0.4 \quad (2)$$

Then, combining both relations we find that the luminosity due to star formation, L_{IR} , has to be at least 20 times brighter than the AGN luminosity (that is, AGN contribution to the total luminosity below 5%) for the star formation to dominate the $[\text{O IV}]25.89\mu\text{m}$ emission.

We note that the number of H II galaxies falls rapidly above $\log L_{[\text{O IV}]} \text{ (erg s}^{-1}) = 40.2$ (see Figure 6). Assuming that star formation dominates the $[\text{O IV}]25.89\mu\text{m}$ emission at this luminosity in these galaxies, the equivalent infrared luminosity (L_{IR}) would be $2 \times 10^{11} L_{\odot}$. This value of the L_{IR} seems reasonable since most of the H II galaxies with $\log L_{[\text{O IV}]} \text{ (erg s}^{-1})$ between 39.6 and 41.0 are classified as LIRGs. The L_{IR} limit calculated above is one order of magnitude larger than L_{\star} (Takeuchi et al. 2003) so the reason for the lower number of H II galaxies above this $[\text{O IV}]25.89\mu\text{m}$ luminosity can be that the space density of luminous star forming galaxies decreases rapidly with increasing luminosity.

Out of 196 galaxies with estimates for L_{IR} , $[\text{O IV}]25.89\mu\text{m}$ is detected in 122. Only $2 \pm 2\%$ of the H II galaxies have $[\text{O IV}]25.89\mu\text{m}$ luminosities 1σ above those expected from their L_{IR} . Likewise star-formation can explain the observed $[\text{O IV}]25.89\mu\text{m}$ luminosities for $9 \pm 4\%$ of the Seyfert galaxies (Figure 7). Thus the $[\text{O IV}]25.89\mu\text{m}$ emission of Seyferts is generally dominated by the AGN, whereas for optically classified H II galaxies star formation is likely to be the origin of the $[\text{O IV}]25.89\mu\text{m}$ emission.

5.2. The $[\text{Ne III}]$ Excess

The $[\text{Ne III}]15.56\mu\text{m}$ emission may be produced by star formation and/or AGN. In this section we try to quantify the contribution of each one to the total $[\text{Ne III}]15.56\mu\text{m}$ output. For this purpose we used the correlations between $[\text{Ne V}]14.32\mu\text{m}$, $[\text{O IV}]25.89\mu\text{m}$ and $[\text{Ne III}]15.56\mu\text{m}$ (see Section 4). Combining the typical $[\text{O IV}]25.89\mu\text{m}/[\text{Ne V}]14.32\mu\text{m}$ and $[\text{Ne III}]15.56\mu\text{m}/[\text{Ne V}]14.32\mu\text{m}$ ratios found in AGN we estimate a ratio $[\text{Ne III}]15.56\mu\text{m}/[\text{O IV}]25.89\mu\text{m} = 0.6$, with rms scatter

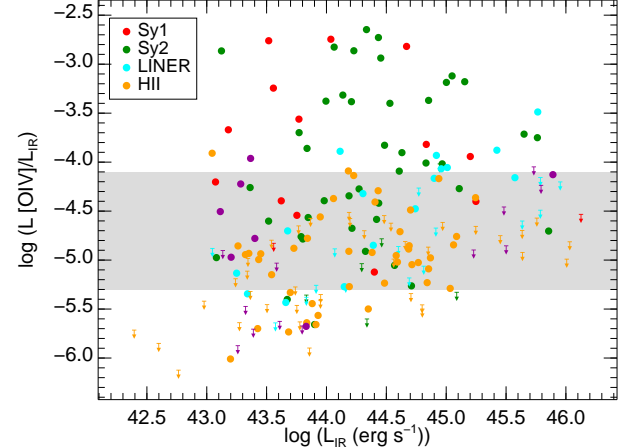


FIG. 7.— $[\text{O IV}]25.89\mu\text{m}/L_{\text{IR}}$ ratio vs. L_{IR} luminosity. Galaxy symbols are as in Figure 2. The shaded region is the upper limit to the $[\text{O IV}]25.89\mu\text{m}/L_{\text{IR}}$ ratio of star-forming galaxies. Galaxies above this region need an AGN contribution to the $[\text{O IV}]25.89\mu\text{m}$ emission in order to explain the observed ratio.

of 0.3 for AGNs⁶, or $\log [\text{Ne III}]/[\text{O IV}] = -0.22$. This estimated ratio is very similar to that obtained using a linear fit between the $[\text{Ne III}]15.56\mu\text{m}$ and $[\text{O IV}]25.89\mu\text{m}$ luminosities (Table 3). The median of this ratio for H II galaxies is 4.7, or $\log [\text{Ne III}]/[\text{O IV}] = 0.67$, which is ~ 8 times larger than that estimated for active galaxies. Figure 8 shows that the observed ratio for Seyfert galaxies and QSOs falls around the predicted value for AGN. Only a small fraction (4%) of the H II galaxies have $[\text{Ne III}]15.56\mu\text{m}/[\text{O IV}]25.89\mu\text{m}$ ratios in the AGN range. It is also apparent that H II galaxies, a large fraction of LINERs and some Seyfert galaxies have an excess of $[\text{Ne III}]15.56\mu\text{m}$ relative to their $[\text{O IV}]25.89\mu\text{m}$ emission which can also be attributed to star formation.

We find that the four H II galaxies with $[\text{Ne V}]14.32\mu\text{m}$ detections have the $[\text{Ne III}]15.56\mu\text{m}/[\text{Ne V}]14.32\mu\text{m}$ and $[\text{Ne II}]12.81\mu\text{m}/[\text{Ne V}]14.32\mu\text{m}$ ratios much larger than those of Seyfert galaxies (Table 3). This indicates that the star-formation contribution is larger than that in Seyfert galaxies. Thus as suggested in Section 2 the AGN does not dominate the nuclear spectra of these galaxies.

As can be seen in the left panel of Figure 4, most of the outliers (galaxies more than 3σ above the $[\text{Ne V}]14.32\mu\text{m}$ versus $[\text{Ne III}]15.56\mu\text{m}$ flux correlation) have $L_{[\text{Ne III}]} < 10^{42} \text{ erg s}^{-1}$. That is, for the most luminous objects the AGN dominates the $[\text{Ne III}]15.56\mu\text{m}$ emission. Using the relation by Ho & Keto (2007) that relates star formation rate (SFR) and the luminosity of the $[\text{Ne II}]12.81\mu\text{m}$ and $[\text{Ne III}]15.56\mu\text{m}$ emission lines and assuming a $[\text{Ne III}]15.56\mu\text{m}/[\text{Ne II}]12.81\mu\text{m}$ ratio = 0.3 (see Section 5.3) we find that the SFR of the outliers is between 0.1 and $100 M_{\odot} \text{ yr}^{-1}$.

5.3. The $[\text{Ne III}]15.56\mu\text{m}/[\text{Ne II}]12.81\mu\text{m}$ Ratio

The $[\text{Ne III}]15.56\mu\text{m}/[\text{Ne II}]12.81\mu\text{m}$ ratio traces the hardness of the radiation field and the age of the stellar population (Rigby & Rieke 2004; Snijders et al. 2007). Figure 9 compares the $[\text{Ne III}]15.56\mu\text{m}/[\text{Ne II}]12.81\mu\text{m}$ ratio observed in H II galaxies (median 0.2) with that

⁶ In this section the term “AGN” refers to galaxies classified as QSO or Seyfert.

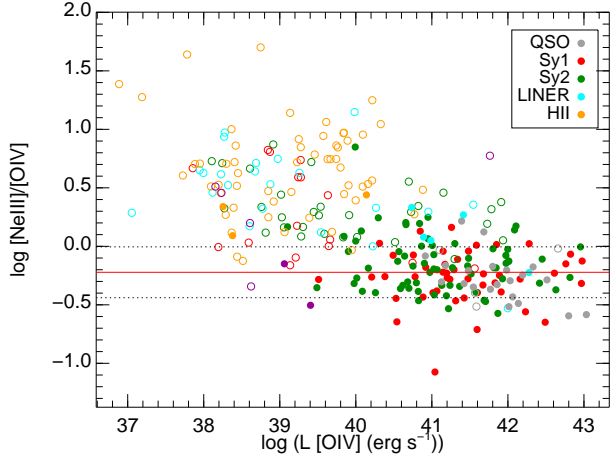


FIG. 8.— $[\text{Ne III}]15.56 \mu\text{m}/[\text{O IV}]25.89 \mu\text{m}$ ratio vs. $[\text{O IV}]25.89 \mu\text{m}$ luminosity. Galaxy symbols are as in Figure 2. The solid red line is the $[\text{O IV}]25.89 \mu\text{m}/[\text{Ne III}]15.56 \mu\text{m}$ ratio calculated from the linear fit to the $[\text{O IV}]25.89 \mu\text{m}$ vs. $[\text{Ne III}]15.56 \mu\text{m}$ luminosities. The dotted black lines are the 1σ deviation.

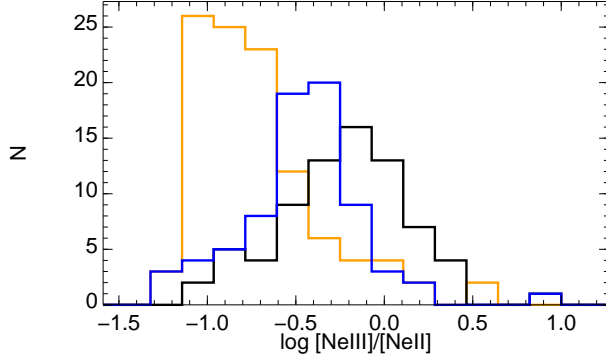


FIG. 9.— Distribution of the $[\text{Ne III}]15.56 \mu\text{m}/[\text{Ne II}]12.81 \mu\text{m}$ ratio. The orange histogram corresponds to the observed ratios in H II galaxies, black corresponds to the observed ratios in active galaxies with star formation ($[\text{Ne III}]15.56 \mu\text{m}/[\text{O IV}]25.89 \mu\text{m}$ ratios > 0.9). The blue histogram shows the ratios calculated for Seyfert galaxies after subtracting the AGN contribution to the $[\text{Ne III}]15.56 \mu\text{m}$ emission.

observed in Seyfert galaxies with star formation⁷ (median 0.6). The larger ratio found in Seyfert galaxies can be explained if the AGN contributes noticeably to the total $[\text{Ne III}]15.56 \mu\text{m}$ emission but not to the $[\text{Ne II}]12.81 \mu\text{m}$ emission (see Section 4.2). By assuming this we calculate the star formation $[\text{Ne III}]15.56 \mu\text{m}/[\text{Ne II}]12.81 \mu\text{m}$ ratio in these Seyfert galaxies using the non-AGN $[\text{Ne III}]15.56 \mu\text{m}$ emission that we estimated using the method described in Section 6. The median of this ratio becomes ~ 0.3 , which is somewhat larger than that found in pure H II galaxies but it is in the range of the observed ratio in this class of galaxies (Brandl et al. 2006).

6. COMPARISON OF STAR FORMATION IN SEYFERT 1 AND 2 GALAXIES

The AGN unification scenario predicts that there should be no differences between the star formation activity in Seyfert 1 and 2 galaxies. A number of studies compared the star formation rates in

Seyfert 1 and 2 galaxies. Some of them found enhanced star formation activity in Seyfert 2 with respect Seyfert 1 galaxies, for a given AGN luminosity (Maiolino et al. 1995; Buchanan et al. 2006; Deo et al. 2007; Meléndez et al. 2008b), whereas others did not find any differences between the two types (Kauffmann et al. 2003; Imanishi & Wada 2004). However, as discussed by Shi et al. (2009), the different methods used to study the star formation activity are sensitive to different stellar age ranges. Therefore these apparently contradictory results may be consistent with each other. The $[\text{Ne III}]15.56 \mu\text{m}$ line is sensitive to young (< 5 Myr) massive star formation (Rigby & Rieke 2004; Snijders et al. 2007). Studies using this line (and the $[\text{Ne II}]12.81 \mu\text{m}$ line) found that star formation is enhanced in Seyfert 2 galaxies (Deo et al. 2007; Meléndez et al. 2008b). Kauffmann et al. (2003) did not find differences between Seyfert 1 and Seyfert 2 star formation, but their method (the 4000Å break and the H δ stellar absorption) was sensitive to stellar populations older than 100 Myr (Shi et al. 2009). The same applies to the PAH features used by Imanishi & Wada (2004), which can be affected by the presence of the AGN (Diamond-Stanic & Rieke 2010, and references therein).

It is also important to use the appropriate indicator for the AGN luminosity. We will use the $[\text{O IV}]25.89 \mu\text{m}$ emission, as it is a good isotropic indicator (Rigby et al. 2009; Diamond-Stanic et al. 2009), as long as the AGN dominates the $[\text{O IV}]25.89 \mu\text{m}$ emission as we showed in Section 5.1.

We estimate the star formation contribution to the $[\text{Ne III}]15.56 \mu\text{m}$ emission by using the observed $[\text{O IV}]25.89 \mu\text{m}/[\text{Ne III}]15.56 \mu\text{m}$ ratio and subtracting the estimated AGN contribution from the total $[\text{Ne III}]15.56 \mu\text{m}$ line strength. Further details are provided in Appendix A. We used the $[\text{O IV}]25.89 \mu\text{m}/[\text{Ne III}]15.56 \mu\text{m}$ instead of the $[\text{O IV}]25.89 \mu\text{m}/[\text{Ne II}]12.81 \mu\text{m}$ ratio because we could not calculate the typical AGN $[\text{O IV}]25.89 \mu\text{m}/[\text{Ne II}]12.81 \mu\text{m}$ ratio due to the larger relative contribution of star formation activity to the $[\text{Ne II}]12.81 \mu\text{m}$ emission (Section 4.2). We only subtract this contribution from those active galaxies more than 1σ above the typical AGN $[\text{Ne III}]15.56 \mu\text{m}/[\text{O IV}]25.89 \mu\text{m}$ ratio (see Section 5.2 and Figure 8), since the galaxies below this ratio are presumably dominated by the AGN and their star formation activity, if any, is masked. This criterion basically selects only those active galaxies with at least 25% of the $[\text{Ne III}]15.56 \mu\text{m}$ emission arising from star formation. In our sample 45% of the AGNs with the $[\text{O IV}]25.89 \mu\text{m}$ line detected have excess $[\text{Ne III}]15.56 \mu\text{m}$ emission due to star formation. The right panel of Figure 10 shows that the fraction of Seyfert 2s with star formation is slightly higher than that of Seyfert 1s. In all the luminosity bins except for one, the difference in the fraction with a $[\text{Ne III}]15.56 \mu\text{m}$ excess is less than 2σ significant. However, for the overall proportion of $[\text{Ne III}]15.56 \mu\text{m}$ excess detections, the Fisher's exact test indicates that there is a probability of less than 0.03 that the incidence of this behavior is the same in the Sy1 and Sy2 samples. Therefore, the full sample in our study supports, with a moderate statistical significance, previous indications that Sy2 host galaxies tend to have higher rates of star

⁷ those with excess $[\text{Ne III}]15.56 \mu\text{m}$.

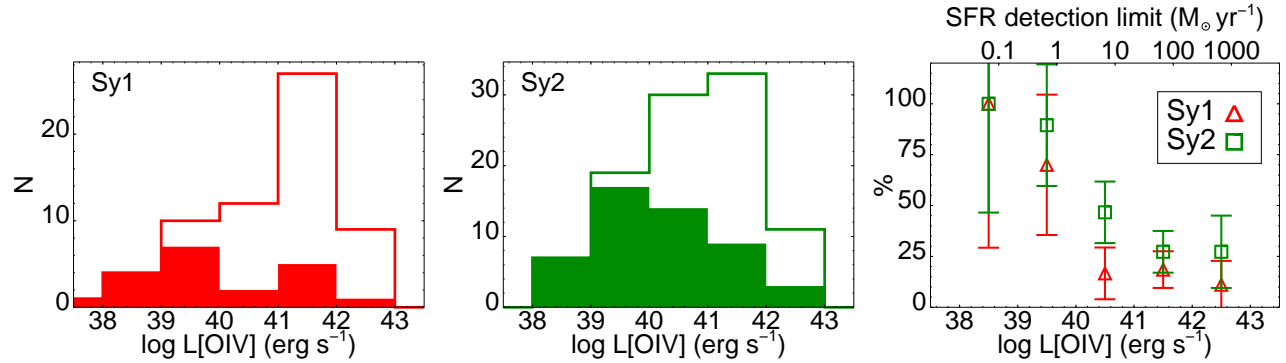


FIG. 10.— Distribution of the [O IV]25.89 μm luminosities of the Seyfert 1 (left) and 2 (middle) galaxies. The filled histograms are the galaxies with a [Ne III]15.56 μm excess. The right panel compares the fraction of type 1 and type 2 Seyferts with a [Ne III]15.56 μm excess for each luminosity bin. We used Poisson statistical errors to estimate the uncertainties of the fractions. The scale on the upper part of the right panel gives the lower limit to the SFR that can be detected with our method for each AGN luminosity bin.

formation than Sy1 hosts. However the full sample is heterogeneous and may be subject to a number of biases. For example, it includes a number of radio galaxies, which are known to have low star formation rates – in fact none of the radio galaxies have [Ne III]15.56 μm excess. It also contains ULIRGs with Seyfert spectral characteristics, most of which do have [Ne III]15.56 μm excess. The observed differences depend to some extent on the relative number of galaxies in these two classes. In the following section, we discuss this trend in two relatively complete but smaller subsamples where the biases should be reduced.

6.1. Results for the 12 μm sample and the RSA samples

At this point we study separately the 12 μm sample and the RSA sample. Both are complete samples of Seyfert galaxies selected with homogeneous criteria. The former is selected based on their *IRAS* 12 μm fluxes whereas the latter is selected based on the optical magnitude of the host galaxy. Given the different selection criteria they might be affected by star formation in different ways.

As can be seen from Table 4 and Figure 11, the fraction of galaxies with a [Ne III]15.56 μm excess in the RSA sample is higher (by a factor of 1.4) than in the 12 μm sample. The lower number of galaxies with a [Ne III]15.56 μm excess in the 12 μm sample is because the galaxies of this sample are brighter and the sensitivity to star formation of our method is reduced at high [O IV]25.89 μm luminosities. Both effects are clearly seen in Figure 11. First, the RSA sample contains a larger fraction of low luminosity Seyferts ($L[\text{O IV}] \leq 10^{40}$ erg s $^{-1}$) than the 12 μm sample. Second, for each AGN luminosity, we are sensitive to a different SFR limit. In other words, for the brightest Seyferts we are only sensitive to SFR above $100 M_{\odot} \text{ yr}^{-1}$, while for low luminosity AGN we are sensitive to SFR $> 0.1 M_{\odot} \text{ yr}^{-1}$. We note that the fraction of galaxies with star formation in each luminosity bin is similar for both samples (right panel of Figure 11).

In both samples the fraction of Seyfert 2s with [Ne III]15.56 μm excess is slightly larger than that of Seyfert 1s. However due to the small size of the samples the statistical significance of this excess is low. Based on the two sample K-S test, the probability for these differences being due to chance is 0.25 and 0.4 for the 12 μm

TABLE 4
FRACTION OF GALAXIES WITH A
[NE III] EXCESS IN THE RSA AND
12 μm SAMPLES

Type	12 μm sample	RSA
Seyfert 1	15/45	12/25
Seyfert 2	23/52	25/45
Total	38/97	37/70

NOTE. — In this table we only include galaxies with the [O IV]25.89 μm and [Ne III]15.56 μm emission lines detected. Some galaxies are common to both samples.

and RSA samples respectively.

7. LINE RATIOS AND MODELS

We studied the physical conditions in the narrow line region of the AGNs with the photoionization code MAP-PINGSIII (Groves et al. 2004). We used a radiation pressure dominated model that includes the effects of dust. For the input parameters we followed the prescription given by Groves et al. (2006). Briefly, we assumed a plane parallel geometry and solar abundances. We modeled the input ionizing spectrum with two power-laws with exponential cut-offs (Nagao et al. 2001). We explored the effect of the variations in the total hydrogen column density ranging from $\log n_{\text{H}} (\text{cm}^{-2}) = 19.0$ to 22.0. This range was chosen since it reproduces the observed line ratios and is in good agreement with the hydrogen column density determined using UV and X-ray observations (Crenshaw et al. 2003). For each hydrogen column density we varied the total pressure (P/k) and the incident ionizing flux (I_0). The values for the total pressure are $\log P/k (\text{K cm}^{-3}) = 6, 7, 8, 9$. These correspond to electron densities, as traced by [S II] $\lambda\lambda 6716\text{\AA}/\lambda 6731\text{\AA}$, of $\sim <10^1, 10^2, 10^3$ and $> 10^4 \text{ cm}^{-3}$ respectively. The explored range for the ionizing flux is $I_0 = 0.1$ to 0.55. The incident ionizing flux is scaled by the factor $2.416 \times ((P/k)/10^6) \text{ erg cm}^{-2} \text{ s}^{-1}$ which gives a range in the ionization parameter, $\log U$, from ~ -3 to -2.

7.1. The [Ne V] ratio

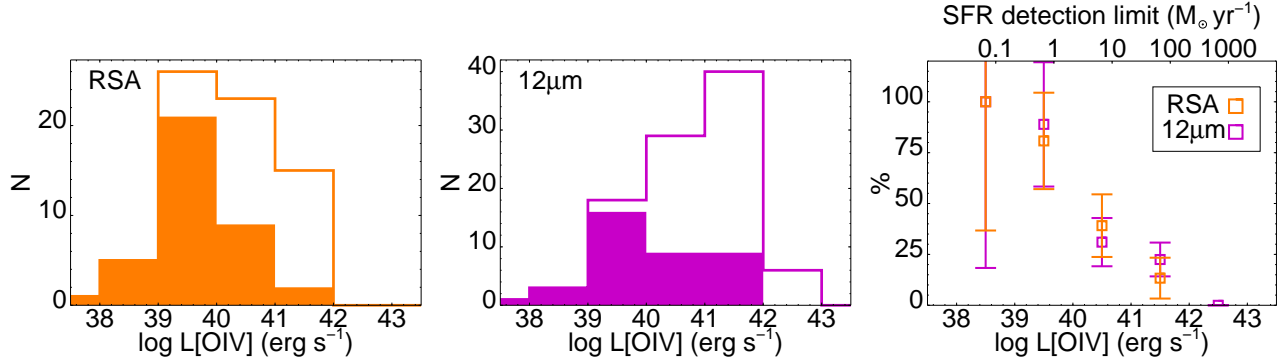


FIG. 11.— Distribution of the [O IV]25.89 μm luminosities for the RSA sample (left panel) and 12 μm sample (middle panel). Symbols are as in Figure 10.

Figure 12 shows the ratio between the two [Ne V] emission lines available in the mid-infrared. The critical densities of the [Ne V]14.32 μm and [Ne V]24.32 μm lines are $3.5 \times 10^4 \text{ cm}^{-3}$ and $6.2 \times 10^3 \text{ cm}^{-3}$, respectively (Osterbrock & Ferland 2006), thus they can be used to trace the density of the NLR. We find however that a large fraction of the galaxies ($\sim 30\%$) lies above the low density limit ratio. This issue and its possible cause are discussed in detail by Dudik et al. (2007) and also addressed by Tommasin et al. (2010) for a sample of Seyfert galaxies. Dudik et al. (2007) concluded that the ratios above the low density limit are due to differential extinction from the obscuring torus, and thus can indicate the inclination angle to our line of sight. However, similar to Baum et al. (2010), we do not find any significant difference between the proportion of Seyfert 1 and Seyfert 2 galaxies above the low density limit, as would be predicted by this hypothesis.

We calculated the $A_{24.3}/A_{14.3}$ ratio to quantify the extinction needed to move the points above the low density limit ratio to this value (which would be a lower limit to the extinction since the real ratio may be lower than the low density limit). The ratios are summarized in Table 5 for some infrared extinction laws. As can be seen depending on the extinction law chosen the extinction can increase or decrease the [Ne V]24.32 μm /[Ne V]14.32 μm ratio. Since the construction of an extinction law implies some interpolation we also used direct measurements of A_{24}/A_K and A_{15}/A_K .⁸ Jiang et al. (2006) measured the extinction at 15 μm and found $A_{15}/A_K = 0.40$, although it ranges from 0.25 to 0.55. For the A_{24}/A_K ratio the range is 0.28 to 0.65 for different A_K bins (Chapman et al. 2009) and the average value is ~ 0.5 (Chapman et al. 2009; Flaherty et al. 2007). From these measurements we estimate $A_{24.3}/A_{14.3} = 1.2 \pm 0.3$. Again it is close to unity and it is not clear if the extinction would increase or decrease the [Ne V] ratio. Moreover the extinction is nearly neutral between the lines with all the extinction laws and therefore there is very little potential effect on the ratio unless the extinction is extremely large.

We also checked if aperture effects can explain the large values of this ratio. The [Ne V]14.32 μm line is observed with the SH module ($5.7 \times 11.3'$), whereas

TABLE 5
EXTINCTION AT 24 μm RELATIVE
TO THAT AT 14 μm

Extinction law	A_{24}/A_{14}
Rosenthal ^a	1.25
McClure $0.3 < A_K < 1$ ^b	0.83
McClure $1 < A_K < 7$ ^b	0.83
Chiar Galactic Center ^c	1.38
Chiar Local ISM ^c	0.97

^a Rosenthal et al. 2000

^b McClure 2009

^c Chiar & Tielens 2006

the [Ne V]24.32 μm is observed with the LH module ($11.1' \times 22.3'$). We would expect a correlation between the [Ne V]24.32 μm /[Ne V]14.32 μm ratio and the distance if the [Ne V] emission region was larger than the SH slit. However we do not find this correlation thus we rule out any aperture bias.

Alternatively the atomic parameters for the Ne⁺⁴ ion may not be sufficiently accurate for the comparison with these observations and the calculated low density limit may be incorrect.

7.2. Ionization parameter

In Figure 12 we plot the model grid together with the data. In this plot we vary the ionizing flux, I_0 , and the total pressure, P/k , for a constant total hydrogen column density ($\log n_{\text{H}} (\text{cm}^{-2}) = 20.3$). We see that the [Ne V] ratio can be used to measure the pressure. However the pressure (or density) values derived from this ratio have some issues, since a considerable fraction of galaxies are above the low density limit ratio (Section 7.1).

Also, Figure 12 shows that the [O IV]25.89 μm /[Ne V]24.32 μm ratio traces the ionization parameter. The [O IV]25.89 μm /[Ne V]24.32 μm ratio spans a narrow range (less than 1 dex) which is related to the tight correlation found between the [O IV]25.89 μm and [Ne V]24.32 μm luminosities (Section 4). This implies a very small range for the ionization parameter ($-2.8 < \log U < -2.5$). This range is similar to that found when modeling the optical [O III] and H β emission (Baskin & Laor 2005; Kraemer et al. 1999). The critical density of the [O III] lines is larger than that of these mid-IR lines and for instance the Baskin & Laor

⁸ From the extinction laws, the difference between these A values and those at 14.3 μm and 24.3 μm would be small ($\sim 5\%$).

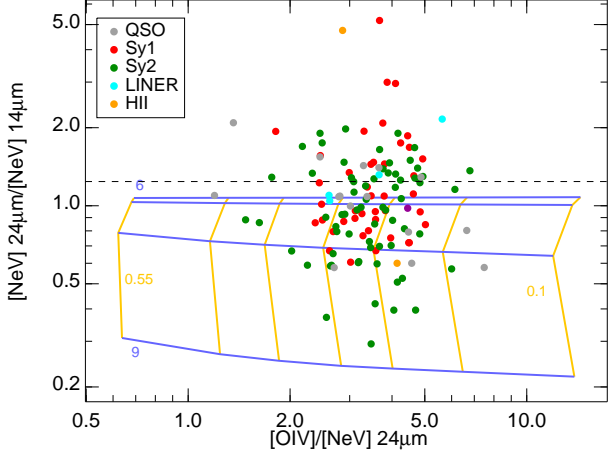


FIG. 12.— Predicted $[\text{Ne V}]24.32 \mu\text{m}/[\text{Ne V}]14.32 \mu\text{m}$ ratio vs. $[\text{O IV}]25.89 \mu\text{m}/[\text{Ne V}]24.32 \mu\text{m}$. Galaxy symbols are as in Figure 2. The dashed black line indicates the low density limit calculated at 10000 K for the $[\text{Ne V}]24.32 \mu\text{m}/[\text{Ne V}]14.32 \mu\text{m}$ ratio (galaxies above this line have densities below the low density limit). The blue lines trace constant pressure and the orange lines constant ionization parameter (I_0). The input parameters for the model are $\log P/k = 6, 7, 8, 9$ and $I_0 = 0.1, 0.15, 0.20, 0.25, 0.32, 0.4, 0.55$ for constant hydrogen column density $\log n_{\text{H}} (\text{cm}^{-2}) = 20.3$. The galaxy symbols are as in Figure 2.

(2005) models predict electron densities $\log n_{\text{e}} (\text{cm}^{-3}) = 5.8 \pm 0.7$ well above the critical density of the mid-IR lines studied here. Thus it is possible that these lines are produced in different gas clouds.

7.3. Hydrogen column density

We use the $[\text{Ne III}]15.56 \mu\text{m}$ and the $[\text{Ne V}]14.32 \mu\text{m}$ lines to estimate the total hydrogen ($\text{H I} + \text{H II}$) column density, n_{H} . The $[\text{Ne V}]14.32 \mu\text{m}$ line is produced in the inner part of the NLR while the $[\text{Ne III}]15.56 \mu\text{m}$ is produced in a more external region. Thus the $[\text{Ne III}]15.56 \mu\text{m}/[\text{Ne V}]14.32 \mu\text{m}$ ratio is subject to change depending on the column density. As expected, the models predict larger $[\text{Ne III}]15.56 \mu\text{m}/[\text{Ne V}]14.32 \mu\text{m}$ ratios for larger n_{H} .

In Figure 13 we plot the model grid together with the observed ratios. The $[\text{Ne III}]15.56 \mu\text{m}/[\text{Ne V}]14.32 \mu\text{m}$ ratio is not sensitive to column densities larger than $\log n_{\text{H}} (\text{cm}^{-2}) > 21$. We find that the column density for most of the galaxies is in the range $20.3 < \log n_{\text{H}} (\text{cm}^{-2}) < 21$. There is no difference between the predicted hydrogen column density for type 1 and 2 galaxies. This column density range is compatible with the values derived from UV observations although lower than that determined using X-ray data (Crenshaw et al. 2003). A few galaxies are above the model grid. The $[\text{Ne III}]15.56 \mu\text{m}/[\text{Ne V}]14.32 \mu\text{m}$ ratio of these galaxies is larger than that predicted by the models. As we proposed in Sections 4.2 and 5.2, star formation acting in these galaxies is likely producing the extra $[\text{Ne III}]15.56 \mu\text{m}$ emission.

8. CONCLUSIONS

We studied a sample of 426 galaxies observed with the *Spitzer*/IRS spectrograph in the high resolution mode. Our analysis includes published data for QSO, Seyfert, LINER and HII galaxies as well as unpublished measurements for the RSA Seyfert sample and LIRGs. We explored the rela-

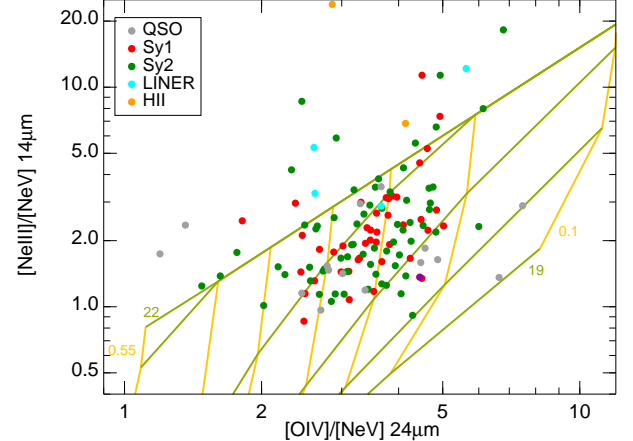


FIG. 13.— Predicted $[\text{Ne III}]15.56 \mu\text{m}/[\text{Ne V}]14.32 \mu\text{m}$ ratio vs. $[\text{O IV}]25.89 \mu\text{m}/[\text{Ne V}]24.32 \mu\text{m}$. The green lines trace constant hydrogen column density and the orange lines constant ionization parameter. The input parameters for the model are $\log n_{\text{H}} (\text{cm}^{-2}) = 19.0, 20.0, 20.3, 20.6, 21.0, 22.0$ and $I_0 = 0.1, 0.15, 0.20, 0.25, 0.32, 0.4, 0.55$ for constant pressure ($\log P/k = 8$). The galaxy symbols are as in Figure 2.

tionship between the high-ionization ($[\text{Ne V}]14.32 \mu\text{m}$, $[\text{Ne V}]24.32 \mu\text{m}$ and $[\text{O IV}]25.89 \mu\text{m}$) and intermediate ionization ($[\text{Ne III}]15.56 \mu\text{m}$ and $[\text{Ne II}]12.81 \mu\text{m}$) emission lines present in the mid-IR spectra. The median ratios for each class of galaxies are listed in Table 3. The main results are as follows:

1. There is a tight linear correlation between the fluxes and luminosities of the high-ionization emission lines $[\text{O IV}]25.89 \mu\text{m}$ and $[\text{Ne V}]24.32 \mu\text{m}$. This correlation spans 5 orders of magnitude ($38 < \log L_{[\text{Ne V}]24} (\text{erg s}^{-1}) < 43$), ranging from LINERS, low-luminosity Seyfert galaxies, types 1 and 2, to QSOs. The typical $[\text{O IV}]25.89 \mu\text{m}/[\text{Ne V}]24.32 \mu\text{m}$ ratio for AGNs is 3.5, with rms scatter of 0.8. The correlation also holds between the $[\text{O IV}]25.89 \mu\text{m}$ and the $[\text{Ne V}]14.32 \mu\text{m}$ lines, although the scatter is larger. The typical $[\text{O IV}]25.89 \mu\text{m}/[\text{Ne V}]14.32 \mu\text{m}$ ratio for AGNs is 3.4, with rms scatter of 1.4.
2. There is also a good linear correlation between the $[\text{Ne III}]15.56 \mu\text{m}$ and the $[\text{Ne V}]14.32 \mu\text{m}$ fluxes and luminosities for Seyfert galaxies and QSO. The $[\text{Ne III}]15.56 \mu\text{m}/[\text{Ne V}]14.32 \mu\text{m}$ ratio is 1.9, with rms scatter of 0.8. Using this correlation and the previous one we calculated the typical $[\text{Ne III}]15.56 \mu\text{m}/[\text{O IV}]25.89 \mu\text{m}$ ratio for AGNs of 0.6, with rms scatter of 0.3.
3. We calculate the $[\text{O IV}]25.89 \mu\text{m}$ emission due to star formation ($\log L_{[\text{O IV}]} (\text{erg s}^{-1}) < \log L_{\text{IR}} (\text{erg s}^{-1}) - 4.7 \pm 0.6$) and we estimate that it may dominate the total $[\text{O IV}]25.89 \mu\text{m}$ emission when the intrinsic AGN luminosity is a factor of 20 smaller than the star forming luminosity. In general, we find that the $[\text{O IV}]25.89 \mu\text{m}$ emission is dominated by the AGN in Seyfert galaxies, whereas star-formation can explain the $[\text{O IV}]25.89 \mu\text{m}$ emission of optically classified HII galaxies.

4. We do not find any significant difference between the mid-IR high-ionization emission lines in type 1 and in type 2 Seyfert galaxies. Either there are no differences in the conditions in the NLR of the two AGN types, or the effects associated with the different line of sight (i.e., dust extinction) are minimized in the mid-infrared spectra.
5. We find that a significant number of Seyfert galaxies from the $12\mu\text{m}$ sample (30%) and the RSA sample (40%) show evidence for excess $[\text{Ne III}]15.56\mu\text{m}$ emission relative to their $[\text{O IV}]25.89\mu\text{m}$ emission associated with star formation. The larger fraction in the RSA sample is explained because the RSA sample contains a larger fraction of low-luminosity AGNs ($L_{[\text{O IV}]} < 10^{41}\text{ erg s}^{-1}$) in which these star formation excesses are easier to detect.
6. The fraction of Seyfert 2 galaxies with $[\text{Ne III}]15.56\mu\text{m}$ excess is larger than that of Seyfert 1 with a moderate statistical significance in the full sample although this sample may be affected by several bias. However when we consider the $12\mu\text{m}$ or RSA Seyfert samples separately these differences are not statistically significant due to the smaller size of these samples.
7. A considerable fraction (30%) of the galaxies have $[\text{Ne V}]24.32\mu\text{m}/[\text{Ne V}]14.32\mu\text{m}$ ratios above the low density limit. We did not find a connection between the Seyfert type and the ratio of galaxies above the limit. We are not able to explain this in terms of differential extinction.
8. Our modeling shows that the nebular conditions in the NLRs are remarkably similar among all the

AGNs in our sample. This similarity allows us to compare conditions critically in the NLRs of the type 1 and type 2 galaxies. There appear to be no significant overall differences, consistent with the unified model. We constrained the ionization parameter in the range $-2.8 < \log U < -2.5$ and the hydrogen column density $20 < \log n_{\text{H}}(\text{cm}^{-2}) < 21$.

The relationships presented in this paper provide an important benchmark for the interpretation of the future mid-IR observations of AGNs and star forming galaxies with JWST/MIRI.

ACKNOWLEDGEMENTS

The authors thank B. Groves and T. Díaz-Santos for their help and enlightening discussion. We thank the anonymous referee for useful comments and suggestions. MP-S acknowledges support from the CSIC under grant JAE-Predoc-2007. MP-S also thanks the Steward Observatory for their hospitality during his stay while part of this work was done. AA-H and MP-S acknowledge support from the Spanish Plan Nacional del Espacio under grant ESP2007-65475-C02-01. This work was partially supported by Caltech/JPL through contract 1255094 to University of Arizona. AA-H also acknowledges support for this work from the Spanish Ministry of Science and Innovation through Proyecto Intramural Especial under grant number 200850I003 and from Plan Nacional de Astronomía y Astrofísica under grant number AYA2009-05705-E. This research has made use of the NASA/IPAC Extragalactic Database (NED) which is operated by the Jet Propulsion Laboratory, California Institute of Technology, under contract with the National Aeronautics and Space Administration. This research also used the VizieR catalogue Service (Ochsenbein et al. 2000).

APPENDIX

A. CALCULATING THE AGN CONTRIBUTION

In this appendix we explain briefly the method used in Sections 5 and 6 to calculate the star formation fraction of the $[\text{Ne III}]15.56\mu\text{m}$ emission.

The total $[\text{Ne III}]15.56\mu\text{m}$ emission includes two components, one from the AGN and other from star formation (SF).

$$[\text{Ne III}] = [\text{Ne III}]_{\text{SF}} + [\text{Ne III}]_{\text{AGN}} \quad (\text{A1})$$

If we assume that all the $[\text{O IV}]25.89\mu\text{m}$ is produced by the AGN we can use the typical $[\text{Ne III}]15.56\mu\text{m}/[\text{O IV}]25.89\mu\text{m}$ ratio observed in Seyfert galaxies with low star formation (Figure 8) to estimate the amount of $[\text{Ne III}]15.56\mu\text{m}$ emission coming from the AGN.

$$[\text{Ne III}] = [\text{Ne III}]_{\text{SF}} + [\text{O IV}] \times \left(\frac{[\text{Ne III}]}{[\text{O IV}]} \right)_{\text{AGN}} \quad (\text{A2})$$

Finally we obtain the fraction of $[\text{Ne III}]15.56\mu\text{m}$ from star formation.

$$\frac{[\text{Ne III}]_{\text{SF}}}{[\text{Ne III}]} = 1 - \frac{[\text{O IV}]}{[\text{Ne III}]} \times \left(\frac{[\text{Ne III}]}{[\text{O IV}]} \right)_{\text{AGN}} \quad (\text{A3})$$

This method can be applied as well to other line ratios. The only assumption is that one of the lines in the ratio is uniquely produced by the AGN while star formation and the AGN contributes to the other line (e.g. the $[\text{Ne III}]15.56\mu\text{m}$ and $[\text{Ne V}]$ lines). Also note that this method makes use of a typical AGN ratio thus the estimated star formation contribution to an emission line for a single object will be uncertain and dependent on the ionization parameter.

TABLE 1
 SAMPLE AND MID-INFRARED EMISSION LINE FLUXES

Name	R.A. ^a (J2000.0)	Decl. ^a (J2000.0)	Dist. ^b (Mpc)	Spect. Class. ^a	[Ne II] 12.81 μ m	[Ne V] 14.32 μ m	[Ne III] 15.56 μ m	[Ne V] 24.32 μ m	[O IV] 25.89 μ m	Ref.
Mrk 335 ^d	00 06 19.5	+20 12 10	113	Sy1	0.25	0.38	0.61	2.0	7.2	4
NGC 23	00 09 53.4	+25 55 25	64.5	H II	96	<0.50	13	<0.44	1.4	2
NGC 24	00 09 56.5	-24 57 47	7.30	...	3.1	<0.88	1.3	...	<0.42	5
Mrk 938 ^d	00 11 06.5	-12 06 26	85.3	Sy2	52	<2.2	6.4	<0.37	<0.66	4
IRAS F00188-0856	00 21 26.5	-08 39 26	600	LINER	4.7	<0.18	0.69	<1.6	<0.90	3
IRAS 00198-7926 ^d	00 21 53.6	-79 10 07	329	Sy2	6.2	12	14	11	33	4
PG 0026+129	00 29 13.6	+13 16 03	672	QSO	0.23	0.47	0.79	<0.33	2.1	1
ESO 012-G021 ^d	00 40 46.2	-79 14 24	144	Sy1	12	3.2	6.4	4.6	16	4
IRAS F00397-1312	00 42 15.5	-12 56 02	1329	H II	4.4	<0.20	2.7	<1.5	<1.2	3
NGC 253	00 47 33.1	-25 17 17	2.50	H II	2832	<21	205	<73	155	8
Mrk 348 ^d	00 48 47.1	+31 57 25	65.1	Sy2	16	5.8	20	4.9	18	4
NGC 278	00 52 04.3	+47 33 01	11.4	...	18	<0.070	3.0	<0.59	<0.62	7
PG 0050+124	00 53 34.9	+12 41 36	273	QSO	1.9	5.5	4.5	<2.1	2.7	1
IRAS 00521-7054 ^d	00 53 56.1	-70 38 04	310	Sy2	5.8	5.8	8.1	2.4	8.6	4
MCG +12-02-001	00 54 03.6	+73 05 11	68.1	H II	242	<1.00	43	<1.4	3.8	2
UGC 556	00 54 50.3	+29 14 47	66.1	H II	40	<0.21	7.1	<0.73	<1.6	2
NGC 337	00 59 50.1	-07 34 40	22.4	H II	19	<0.74	8.0	...	<0.49	5
ESO 541-IG012 ^d	01 02 17.5	-19 40 08	253	Sy2	1.9	2.2	2.0	1.2	5.0	4
IRAS 01003-2238	01 02 50.0	-22 21 57	550	H II	3.1	<0.30	1.3	<0.30	<0.30	3
3C 33	01 08 52.9	+13 20 13	269	Sy2	3.9	2.0	5.3	...	8.1	6
NGC 404	01 09 27.0	+35 43 04	3.24	LINER	3.1	<0.16	1.7	<0.31	0.90	2
NGC 424 ^d	01 11 27.6	-38 05 00	50.8	Sy2	8.7	16	18	6.4	26	4
NGC 526A ^d	01 23 54.4	-35 03 55	83.0	Sy1	5.8	6.3	10	5.9	19	4
NGC 513 ^d	01 24 26.9	+33 47 58	85.0	Sy2	13	1.9	4.4	1.1	6.5	4
NGC 520	01 24 35.1	+03 47 32	30.2	H II	45	<0.64	7.5	<1.4	8.1	8
NGC 584	01 31 20.8	-06 52 05	20.0	<0.92	1.7	...	<0.30	5
NGC 613	01 34 18.2	-29 25 06	15.0	H II	131	0.67	16	3.2	9.1	7
NGC 633	01 36 23.4	-37 19 17	74.2	H II	50	<0.50	6.1	<0.59	1.9	2
NGC 628	01 36 41.8	+15 47 00	7.30	...	6.2	<1.00	<0.38	5
IRAS 01364-1042	01 38 52.9	-10 27 11	215	H II	7.9	<0.32	1.5	<0.60	<0.91	2
NGC 660	01 43 02.4	+13 38 42	12.1	H II	346	<0.57	37	<4.5	28	2
Mrk 573	01 43 57.8	+02 20 59	73.8	Sy2	...	18	24	...	<79	6
III Zw 035	01 44 30.5	+17 06 05	120	...	3.8	<0.17	0.19	<1.9	<1.3	2
IRAS 01475-0740 ^d	01 50 02.7	-07 25 48	76.7	Sy2	14	6.4	9.9	1.9	6.5	4
3C 55	01 57 10.5	+28 51 37	4522	Sy2	...	1.1	2.0	6
Mrk 1014	01 59 50.2	+00 23 40	781	Sy1	6.6	7.4	9.7	5.0	13	3
NGC 788 ^c	02 01 06.4	-06 48 55	58.9	Sy2	6.1	5.3	14	7.9	23	2
NGC 855	02 14 03.6	+27 52 37	9.60	...	5.5	<0.72	<0.40	5
NGC 891	02 22 33.4	+42 20 56	8.60	H II	8.6	<0.040	0.84	<0.62	<1.0	7
Mrk 1034 NED01 ^d	02 23 18.9	+32 11 18	148	Sy1	19	<1.1	1.5	<0.59	<0.77	4
Mrk 1034 NED02 ^d	02 23 22.0	+32 11 49	148	Sy1	35	1.1	3.6	<0.60	2.7	4
UGC 1845	02 24 08.0	+47 58 11	66.7	H II	106	<0.59	11	<0.82	3.1	2
ESO 545-G013 ^d	02 24 40.6	-19 08 31	148	Sy1	10	4.8	11	3.2	12	4
NGC 925	02 27 16.9	+33 34 45	9.10	H II	10	<1.0	5.1	...	<0.36	5
NGC 931 ^d	02 28 14.5	+31 18 41	72.2	Sy1	5.5	14	15	14	43	4
NGC 1055	02 41 45.2	+00 26 35	11.3	Sy2	26	<0.19	2.6	<0.58	1.2	7
NGC 1068 ^{c d}	02 42 40.7	-00 04 47	16.3	Sy2	461	895	1355	808	2061	2
NGC 1056 ^d	02 42 48.3	+28 34 27	22.1	Sy2	34	<1.8	10	<1.2	1.4	4
NGC 1058 ^c	02 43 30.0	+37 20 28	7.42	Sy2	1.0	<0.46	...	<0.33	<0.50	2
UGC 2238	02 46 17.5	+13 05 44	94.5	H II	65	<0.47	10	<2.6	5.5	2
NGC 1097 ^{c d}	02 46 19.1	-30 16 29	17.7	Sy1	165	<0.74	20	<2.4	5.0	2
IRAS 02438+2122	02 46 39.1	+21 35 10	102	LINER	18	<0.33	1.6	<2.2	<2.6	2
NGC 1125 ^d	02 51 40.3	-16 39 03	47.2	Sy2	16	5.1	16	9.7	40	4
NGC 1142 ^d	02 55 12.2	-00 11 00	126	Sy2	17	0.92	5.4	1.8	5.3	4
Mrk 1066	02 59 58.6	+36 49 14	51.9	Sy2	...	18	52	6
MCG -02-08-039 ^d	03 00 30.6	-11 24 56	131	Sy2	3.9	6.6	9.8	5.2	14	4
NGC 1194 ^d	03 03 49.1	-01 06 13	58.9	Sy2	3.8	4.3	7.4	3.8	15	4
NGC 1204	03 04 39.9	-12 20 28	64.8	H II	54	<0.34	5.0	<2.0	<1.6	2
NGC 1222	03 08 56.7	-02 57 18	32.3	H II	81	<0.57	89	<0.78	9.9	8
3C 79	03 10 00.1	+17 05 58	1295	Sy2	...	0.11	0.20	...	0.70	6
NGC 1241 ^{c d}	03 11 14.6	-08 55 19	58.5	Sy2	14	2.5	8.4	1.5	4.8	2
NGC 1266	03 16 00.8	-02 25 38	30.0	LINER	29	<0.92	9.7	...	<1.4	5
NGC 1291	03 17 18.6	-41 06 29	10.8	H II	5.2	<0.86	7.2	...	1.4	5
IRAS F03158+4227	03 19 12.4	+42 38 28	631	...	5.8	<1.1	0.94	<1.4	<1.8	3
NGC 1275 ^c	03 19 48.2	+41 30 42	76.2	Sy2	43	<1.2	21	<2.5	9.6	2
NGC 1316	03 22 41.7	-37 12 29	24.3	LINER	13	<0.61	11	...	2.6	5
NGC 1320 ^d	03 24 48.7	-03 02 32	38.3	Sy2	9.6	11	14	7.5	27	4
NGC 1365 ^{c d}	03 33 36.4	-36 08 25	23.9	Sy1	156	19	61	40	151	2
NGC 1358 ^c	03 33 39.7	-05 05 21	58.2	Sy2	5.1	3.5	8.2	<1.6	9.1	2
NGC 1377	03 36 39.1	-20 54 08	25.2	H II	4.1	<1.9	2.6	...	<1.7	5
NGC 1386 ^{c d}	03 36 46.2	-35 59 57	12.5	Sy2	14	37	39	34	97	2
NGC 1404	03 38 51.9	-35 35 39	18.5	...	1.4	<0.97	1.00	...	<0.35	5
NGC 1433 ^{c d}	03 42 01.6	-47 13 19	15.4	Sy2	...	<1.6	...	<1.9	<6.9	2
NGC 1448	03 44 31.9	-44 38 41	11.5	...	8.2	3.7	5.0	3.6	16	7
IC 342	03 46 48.5	+68 05 46	4.60	H II	615	<2.4	37	<4.9	<7.7	8

TABLE 1 — *Continued*

Name	R.A. ^a (J2000.0)	Decl. ^a (J2000.0)	Dist. ^b (Mpc)	Spect. Class. ^a	[Ne II] 12.81 μm	[Ne V] 14.32 μm	[Ne III] 15.56 μm	[Ne V] 24.32 μm	[O IV] 25.89 μm	Ref.
IRAS 03450+0055 ^{c d}	03 47 40.2	+01 05 14	136	Sy1	1.1	<1.5	1.8	<1.9	2.5	4
NGC 1482	03 54 38.9	-20 30 08	23.2	H II	457	<2.6	56	...	<6.4	5
IRAS 03521+0028	03 54 42.2	+00 37 03	724	LINER	2.8	<0.45	1.3	<0.48	<0.90	3
NGC 1512	04 03 54.3	-43 20 55	11.8	H II	31	<1.1	4.7	...	<0.83	5
3C 109	04 13 40.4	+11 12 13	1589	Sy1	0.030	0.070	0.11	...	0.27	6
IC 2056	04 16 24.5	-60 12 24	13.8	...	13	<0.16	2.2	<0.10	0.75	7
NGC 1559	04 17 35.8	-62 47 01	12.7	...	15	<0.44	2.3	<0.36	<0.69	7
NGC 1566 ^{c d}	04 20 00.4	-54 56 16	21.3	Sy1	15	1.1	9.6	<1.9	8.4	2
NGC 1569	04 30 49.1	+64 50 52	4.60	Sy1	19	<0.38	188	<1.4	29	7
3C 120 ^d	04 33 11.1	+05 21 15	145	Sy1	7.8	17	28	29	123	4
Mrk 618 ^d	04 36 22.2	-10 22 33	156	Sy1	16	3.9	5.4	<1.3	10	4
IRAS F04385–0828 ^d	04 40 55.0	-08 22 22	65.4	Sy2	14	2.3	7.1	<1.4	8.6	4
NGC 1667 ^{c d}	04 48 37.1	-06 19 11	65.9	Sy2	10.0	<0.32	6.9	1.7	6.3	2
NGC 1705	04 54 13.5	-53 21 39	5.10	H II	3.2	<0.91	12	...	2.5	5
ESO 033-G002 ^d	04 55 59.0	-75 32 28	78.6	Sy2	2.1	6.3	9.2	5.3	14	4
NGC 1792	05 05 14.4	-37 58 50	12.5	H II	23	0.41	2.1	<0.25	0.96	7
NGC 1808	05 07 42.3	-37 30 47	12.6	Sy2	177	<0.91	17	<8.4	<9.5	7
ESO 362-G018 ^d	05 19 35.8	-32 39 27	53.8	Sy1	12	3.3	7.5	2.6	8.9	4
IRAS F05189–2524	05 21 01.5	-25 21 45	190	Sy2	21	18	18	12	24	3
IRAS 05187–1017	05 21 06.5	-10 14 46	126	LINER	10	<0.15	1.9	<0.66	<0.92	2
ESO 253-G003 ^d	05 25 18.1	-46 00 21	188	Sy2	16	6.8	18	7.2	24	4
UGC 3351	05 45 47.9	+58 42 03	64.1	H II	67	<0.50	9.6	<0.31	0.83	2
UGCA 116	05 55 42.6	+03 23 31	11.6	H II	6.0	<0.28	117	<1.1	8.5	7
IRAS F05563–3820 ^d	05 58 02.0	-38 20 04	149	Sy1	3.9	2.5	4.8	<0.79	5.3	4
IRAS F06035–7102	06 02 54.0	-71 03 10	358	H II	7.0	<0.48	1.7	<0.81	<3.0	3
ESO 121-G006	06 07 29.9	-61 48 27	14.5	...	16	0.65	3.2	<0.59	4.6	7
Mrk 3	06 15 36.4	+71 02 15	60.6	Sy2	100	64	179	...	214	6
NGC 2146	06 18 37.7	+78 21 25	16.5	H II	625	<2.8	91	<3.7	19	8
UGC A 127	06 20 55.7	-08 29 44	10.2	...	9.3	<0.15	1.5	<0.97	3.4	7
IRAS F06206–6315	06 21 01.2	-63 17 23	421	Sy2	6.6	2.3	2.9	2.0	3.0	3
NGC 2273 ^c	06 50 08.7	+60 50 44	26.5	Sy2	40	4.5	19	6.1	14	2
Mrk 6 ^d	06 52 12.3	+74 25 37	81.7	Sy1	28	9.4	49	10	48	4
IRAS 07145–2914	07 16 31.2	-29 19 28	25.8	Sy2	...	83	168	6
NGC 2369	07 16 37.7	-62 20 37	46.2	H II	124	<0.51	10	<0.91	1.8	2
NGC 2388	07 28 53.4	+33 49 08	58.9	H II	121	<1.2	9.8	<0.79	1.4	2
MCG +02-20-003	07 35 43.4	+11 42 33	71.1	H II	60	<0.47	6.3	<0.53	<1.2	2
NGC 2403	07 36 51.4	+65 36 09	3.20	H II	5.1	<0.71	2.1	...	<0.36	5
Mrk 9 ^d	07 36 57.0	+58 46 13	176	Sy1	3.2	2.2	1.9	2.2	5.6	4
3C 184	07 39 24.5	+70 23 10	6559	Sy2	0.19	0.17	0.65	6
Mrk 79 ^d	07 42 32.8	+49 48 34	96.7	Sy1	10	6.6	20	13	42	4
ESO 209-G009	07 58 15.4	-49 51 15	11.8	...	9.8	<0.26	1.4	<0.12	<0.29	7
IRAS F07598+6508	08 04 33.1	+64 59 48	703	...	3.9	<0.75	2.5	<3.0	<1.8	3
3C 196	08 13 36.0	+48 13 02	5572	Sy1	...	0.30	0.46	6
IRAS 08311–2459	08 33 20.6	-25 09 33	460	Sy1	24	12	23	9.8	26	3
UGC 4459	08 34 07.2	+66 10 54	2.78	<0.89	0.98	...	<0.37	5
NGC 2623	08 38 24.1	+25 45 16	77.4	Sy2	56	2.7	15	2.2	9.6	8
NGC 2639 ^{c d}	08 43 38.1	+50 12 20	44.6	Sy1	8.9	<0.45	4.9	<0.82	1.8	2
PG 0838+770	08 44 45.3	+76 53 09	615	QSO	0.41	0.32	0.56	<0.19	1.3	1
PG 0844+349	08 47 42.5	+34 45 04	287	QSO	0.42	0.30	1.0	0.42	1.5	1
NGC 2681	08 53 32.7	+51 18 49	12.5	...	6.9	<0.15	3.4	<0.36	2.2	7
NGC 2685 ^c	08 55 34.7	+58 44 03	12.7	Sy2	...	<0.28	...	<0.22	0.43	2
NGC 2655 ^{c d}	08 55 37.7	+78 13 23	20.2	Sy2	13	<1.3	7.2	<1.3	<8.0	2
IRAS F08572+3915	09 00 25.4	+39 03 54	259	...	7.2	<0.75	2.0	<5.4	<6.0	3
IRAS 09022–3615	09 04 12.7	-36 27 01	269	...	57	<2.4	40	<3.6	6.7	3
NGC 2798	09 17 22.9	+41 59 59	26.2	H II	215	<1.9	33	...	<5.1	5
Mrk 704 ^d	09 18 26.0	+16 18 19	128	Sy1	...	3.9	5.6	<3.7	12	4
NGC 2841	09 22 02.6	+50 58 35	14.1	LINER	5.7	<4.5	6.7	...	0.78	5
NGC 2915	09 26 11.5	-76 37 34	3.80	H II	3.2	<0.75	11	...	0.45	5
NGC 2903	09 32 10.1	+21 30 03	8.30	H II	182	<0.82	14	<0.94	<1.7	7
UGC 5101	09 35 51.7	+61 21 11	172	LINER	34	2.6	14	2.8	7.3	3
NGC 2992 ^{c d}	09 45 42.1	-14 19 34	33.2	Sy2	46	22	61	28	131	2
NGC 2976	09 47 15.5	+67 54 59	3.60	H II	7.4	<0.99	2.8	...	<0.31	5
NGC 3059	09 50 08.2	-73 55 19	14.2	...	27	<0.18	3.1	<0.69	<1.5	7
Mrk 1239 ^d	09 52 19.1	-01 36 43	86.7	Sy1	9.4	3.4	9.4	3.2	16	4
NGC 3049	09 54 49.6	+09 16 15	23.9	H II	39	<0.89	6.0	...	<1.00	5
NGC 3031 ^{c d}	09 55 33.2	+69 03 55	3.64	Sy1	27	<0.50	21	<1.4	4.5	2
M 82	09 55 52.7	+69 40 45	3.60	H II	506	<0.89	81	<15	46	7
Holmberg IX	09 57 32.0	+69 02 45	2.64	<0.64	<0.38	5
NGC 3081 ^c	09 59 29.5	-22 49 34	34.3	Sy2	12	30	34	39	118	2
3C 234 ^d	10 01 49.5	+28 47 08	897	Sy2	...	2.3	3.4	2.9	9.0	4
NGC 3079 ^{c d}	10 01 57.8	+55 40 47	16.2	Sy2	108	0.91	24	<0.89	11	2
NGC 3110	10 04 02.1	-06 28 29	72.4	H II	75	<0.68	9.9	<0.62	1.2	2
PG 1001+054	10 04 20.1	+05 13 00	771	QSO	0.40	<0.21	0.21	<0.30	0.52	1
NGC 3175	10 14 42.1	-28 52 19	13.4	H II	34	<0.35	2.5	<0.86	1.1	7
IC 2560 ^c	10 16 18.7	-33 33 49	41.7	Sy2	16	19	36	18	56	2
NGC 3147 ^{c d}	10 16 53.7	+73 24 02	40.3	Sy2	4.5	<0.59	3.4	<0.91	<2.5	2
NGC 3185 ^c	10 17 38.6	+21 41 17	17.7	Sy2	9.6	1.0	3.6	1.8	8.2	2

TABLE 1 — *Continued*

Name	R.A. ^a (J2000.0)	Decl. ^a (J2000.0)	Dist. ^b (Mpc)	Spect. Class. ^a	[Ne II] 12.81 μm	[Ne V] 14.32 μm	[Ne III] 15.56 μm	[Ne V] 24.32 μm	[O IV] 25.89 μm	Ref.
NGC 3190	10 18 05.6	+21 49 55	20.9	LINER	8.3	<0.67	4.8	...	0.93	5
NGC 3184	10 18 17.0	+41 25 27	11.1	H II	18	<0.83	2.2	...	<0.29	5
NGC 3198	10 19 54.9	+45 32 59	13.7	...	15	<1.00	0.81	...	<0.32	5
NGC 3227 ^{c d}	10 23 30.6	+19 51 54	15.7	Sy1	66	23	74	18	70	2
NGC 3245	10 27 18.4	+28 30 26	18.2	H II	9.9	<0.21	3.0	<0.76	0.71	2
NGC 3256	10 27 51.3	-43 54 13	40.1	H II	780	<1.9	119	<7.9	<20	2
NGC 3265	10 31 06.8	+28 47 48	23.2	H II	30	<0.78	5.4	...	<0.71	5
NGC 3281 ^c	10 31 52.1	-34 51 13	49.6	Sy2	17	47	58	46	173	2
Mrk 33	10 32 31.9	+54 24 03	22.9	H II	59	<1.0	45	...	0.89	5
3C 244.1	10 33 34.0	+58 14 35	2353	Sy2	1.4	0.60	0.30	6
NGC 3310	10 38 45.9	+53 30 12	19.8	H II	28	<0.25	28	<1.0	4.0	8
IRAS 10378+1109	10 40 29.2	+10 53 18	641	LINER	3.5	<1.1	0.60	<2.4	2.0	3
NGC 3351	10 43 57.7	+11 42 13	9.30	H II	219	<2.3	18	...	2.5	5
NGC 3368	10 46 45.7	+11 49 11	10.5	LINER	4.3	<0.29	2.8	<0.74	0.99	7
NGC 3393	10 48 23.5	-25 09 43	56.2	Sy2	...	42	95	6
IRAS F10565+2448	10 59 18.1	+24 32 34	190	H II	64	<1.00	7.6	<0.90	<1.2	3
NGC 3511 ^d	11 03 23.8	-23 05 12	15.9	Sy1	8.7	<0.49	1.00	<1.7	<1.8	4
NGC 3507	11 03 25.4	+18 08 07	14.2	LINER	3.7	<0.12	1.4	<0.55	<0.21	2
3C 249.1	11 04 13.7	+76 58 58	1619	Sy1	...	0.090	0.14	...	<0.23	6
NGC 3521	11 05 48.6	-00 02 09	10.1	H II	14	<0.95	7.4	...	2.2	5
NGC 3516 ^{c d}	11 06 47.5	+72 34 06	38.0	Sy1	7.2	7.3	16	9.5	44	2
ESO 265-G007	11 07 49.6	-46 31 27	11.7	...	2.6	<0.41	1.1	<1.2	<1.0	7
NGC 3556	11 11 31.0	+55 40 26	13.9	H II	21	<0.37	3.2	<1.2	<1.5	8
IRAS F11095-0238	11 12 03.4	-02 54 22	495	LINER	6.1	<0.48	1.9	<1.8	<0.90	3
IRAS F11119+3257	11 14 38.9	+32 41 33	920	Sy1	3.0	0.75	2.0	<0.90	1.9	3
NGC 3621	11 18 16.5	-32 48 50	6.60	H II	16	1.0	5.7	...	4.6	5
NGC 3627	11 20 15.0	+12 59 29	9.40	Sy2	23	<0.92	8.5	...	1.7	5
NGC 3628	11 20 17.0	+13 35 22	10.00	LINER	126	0.90	10	<1.0	<2.4	8
MCG +00-29-023 ^d	11 21 12.3	-02 59 03	109	Sy2	47	<1.0	4.4	<5.4	<6.0	4
PG 1119+120	11 21 47.1	+11 44 18	222	QSO	0.46	1.7	2.7	1.3	5.9	1
NGC 3642	11 22 17.9	+59 04 28	22.3	LINER	2.8	<0.11	0.97	<0.54	<0.18	2
NGC 3660 ^d	11 23 32.3	-08 39 30	53.1	Sy2	6.5	0.98	1.5	1.7	3.6	4
IRAS 11215-2806 ^c	11 24 02.8	-28 23 15	59.5	Sy2	1.5	2.6	5.2	2.8	12	2
NGC 3675	11 26 08.6	+43 35 09	12.7	H II	8.1	<0.23	2.2	<0.48	<0.58	7
IC 694	11 28 27.3	+58 34 42	44.5	H II	294	<1.6	69	<4.7	<19	2
NGC 3690	11 28 32.2	+58 33 44	44.0	Sy2	151	<1.5	77	<4.6	21	2
PG 1126-041	11 29 16.7	-04 24 07	269	QSO	1.4	4.3	5.2	4.7	16	1
NGC 3726	11 33 21.1	+47 01 45	14.5	H II	5.5	<0.41	0.43	<0.52	<0.44	7
NGC 3735 ^{c d}	11 35 57.3	+70 32 08	38.9	Sy2	9.4	7.1	13	9.8	37	2
NGC 3773	11 38 12.9	+12 06 43	11.9	H II	18	<0.81	16	...	0.36	5
NGC 3783 ^c	11 39 01.7	-37 44 18	41.6	Sy1	18	16	27	12	40	2
NGC 3884	11 46 12.2	+20 23 29	101	LINER	1.5	<0.12	0.86	<0.72	<0.72	2
NGC 3898	11 49 15.4	+56 05 03	16.1	H II	1.0	<0.13	1.3	<0.51	0.40	2
NGC 3938	11 52 49.5	+44 07 14	13.3	H II	5.4	<0.66	1.0	...	0.25	5
ESO 320-G030	11 53 11.7	-39 07 48	43.6	H II	110	<0.53	11	<1.6	<0.88	2
NGC 3949	11 53 41.7	+47 51 31	13.6	H II	5.8	<0.11	1.1	<0.11	1.5	7
NGC 3976 ^c	11 55 57.6	+06 45 02	36.0	Sy2	2.3	<0.26	1.1	<0.35	0.73	2
NGC 3982 ^{c d}	11 56 28.1	+55 07 30	15.2	Sy2	9.2	3.0	6.7	1.7	4.6	2
NGC 3998	11 57 56.1	+55 27 12	14.6	LINER	11	<0.18	6.9	<0.65	0.74	2
NGC 4013	11 58 31.4	+43 56 47	13.8	H II	13	<0.090	2.8	<0.89	<1.0	7
NGC 4036	12 01 26.8	+61 53 44	19.1	LINER	4.4	<0.060	2.8	<0.37	1.4	2
NGC 4051 ^{c d}	12 03 09.6	+44 31 52	9.27	Sy1	17	11	16	10	32	2
IRAS F12018+1941	12 04 24.5	+19 25 09	813	LINER	3.0	<0.80	0.35	<0.10	<0.63	3
NGC 4085	12 05 22.7	+50 21 10	14.6	H II	23	<0.15	2.9	<0.92	<0.44	7
NGC 4088	12 05 34.2	+50 32 20	13.4	H II	37	<0.39	2.5	<0.50	0.73	8
NGC 4125	12 08 06.0	+65 10 26	22.9	LINER	2.3	<0.62	3.3	...	0.75	5
IRAS 12071-0444	12 09 45.1	-05 01 13	600	Sy2	5.2	2.9	5.1	3.7	6.6	3
NGC 4151 ^{c d}	12 10 32.6	+39 24 20	14.0	Sy1	131	77	205	68	244	2
NGC 4157	12 11 04.4	+50 29 04	13.3	H II	12	<0.070	1.4	<0.70	1.1	7
NGC 4192	12 13 48.3	+14 54 01	19.3	H II	19	<0.18	4.7	<0.48	1.6	2
NGC 4194	12 14 09.5	+54 31 36	40.3	Sy2	165	3.0	54	4.0	27	8
PG 1211+143	12 14 17.7	+14 03 12	368	QSO	0.32	<0.43	0.73	<0.56	2.4	1
NGC 4236	12 16 42.1	+69 27 45	4.36	<1.5	<0.23	5
NGC 4235 ^c	12 17 09.9	+07 11 29	33.5	Sy1	3.8	<0.43	3.3	<0.54	3.3	2
Mrk 766 ^d	12 18 26.5	+29 48 46	55.9	Sy1	23	21	24	18	46	4
NGC 4254	12 18 49.6	+14 24 59	16.6	H II	53	<0.92	6.1	...	2.5	5
NGC 4258 ^c	12 18 57.5	+47 18 14	6.60	Sy1	12	<1.3	8.1	<0.82	7.5	2
NGC 4278	12 20 06.8	+29 16 50	9.17	LINER	5.4	<0.23	3.9	<0.29	0.88	2
NGC 4321	12 22 54.9	+15 49 20	14.3	LINER	152	<1.2	18	...	<1.9	5
Mrk 52	12 25 42.8	+00 34 21	30.1	H II	29	<0.57	3.8	<0.83	1.3	8
NGC 4388 ^{c d}	12 25 46.7	+12 39 43	36.3	Sy2	75	45	106	68	308	2
NGC 4395 ^c	12 25 48.9	+33 32 48	4.33	Sy1	4.9	0.93	6.8	1.4	6.9	2
NGC 4419	12 26 56.4	+15 02 50	17.2	H II	36	<0.46	8.5	<1.0	<1.6	2
NGC 4435	12 27 40.5	+13 04 44	11.9	H II	6.8	<0.24	2.1	<0.67	1.1	2
NGC 4450	12 28 29.6	+17 05 05	16.6	LINER	3.5	<0.53	2.1	...	0.63	5
NGC 4457	12 28 59.0	+03 34 14	12.4	LINER	7.8	<0.18	3.2	<0.47	2.2	2
3C 273	12 29 06.7	+02 03 08	755	Sy1	1.5	3.4	6.0	2.9	8.5	3
NGC 4477 ^c	12 30 02.2	+13 38 11	19.3	Sy2	3.2	<0.33	2.8	<3.5	1.3	2

TABLE 1 — *Continued*

Name	R.A. ^a (J2000.0)	Decl. ^a (J2000.0)	Dist. ^b (Mpc)	Spect. Class. ^a	[Ne II] 12.81 μm	[Ne V] 14.32 μm	[Ne III] 15.56 μm	[Ne V] 24.32 μm	[O IV] 25.89 μm	Ref.
NGC 4490	12 30 36.4	+41 38 37	10.5	...	3.5	<0.10	3.5	<0.10	1.1	7
NGC 4486	12 30 49.4	+12 23 28	17.0	Sy2	6.9	<0.19	5.4	<0.57	1.2	2
NGC 4501 ^{c d}	12 31 59.2	+14 25 13	32.7	Sy2	5.0	<0.47	4.7	<0.43	2.5	2
PG 1229+204	12 32 03.6	+20 09 29	283	QSO	0.61	0.91	1.3	0.99	2.8	1
NGC 4536	12 34 27.1	+02 11 17	14.4	H II	386	<1.2	60	...	<7.9	5
NGC 4507 ^c	12 35 36.6	-39 54 33	50.9	Sy2	30	12	29	8.6	34	2
NGC 4552	12 35 39.8	+12 33 22	15.9	LINER	1.7	<0.89	2.9	...	<0.53	5
NGC 4559	12 35 57.7	+27 57 35	10.3	H II	8.3	<1.0	2.3	...	0.12	5
NGC 4565 ^{c d}	12 36 20.8	+25 59 15	18.1	Sy1	2.6	0.32	3.3	<0.82	4.1	2
NGC 4569	12 36 49.8	+13 09 46	16.6	LINER	36	<0.93	16	...	2.9	5
NGC 4579 ^{c d}	12 37 43.5	+11 49 05	21.5	Sy1	23	<0.40	12	<0.68	3.2	2
NGC 4593 ^{c d}	12 39 39.4	-05 20 39	38.8	Sy1	6.8	3.5	7.4	5.4	13	2
NGC 4594 ^{c d}	12 39 59.4	-11 37 23	15.7	Sy1	14	<0.55	16	<0.71	2.4	2
NGC 4602 ^d	12 40 36.9	-05 07 58	36.5	Sy1	7.6	0.82	0.63	<1.2	<2.3	4
TOL 1238-364 ^{c d}	12 40 52.9	-36 45 21	47.7	Sy2	42	9.0	27	3.5	17	2
NGC 4625	12 41 52.7	+41 16 26	9.20	...	5.9	<0.84	1.2	...	<0.26	5
NGC 4631	12 42 08.0	+32 32 29	8.10	H II	133	<0.52	30	...	3.0	5
NGC 4639 ^c	12 42 52.4	+13 15 26	14.0	Sy1	0.84	<0.27	1.1	<0.28	<1.2	2
NGC 4666	12 45 08.6	-00 27 42	21.5	LINER	35	<0.30	8.3	1.4	6.3	2
NGC 4676	12 46 10.1	+30 43 55	94.0	H II	28	<0.25	4.7	<0.33	1.4	8
PG 1244+026	12 46 35.2	+02 22 08	213	QSO	0.94	0.53	1.2	1.1	1.5	1
NGC 4725 ^{c d}	12 50 26.6	+25 30 03	17.4	Sy2	1.2	<0.38	2.4	<0.50	1.8	2
NGC 4736	12 50 53.1	+41 07 13	5.00	LINER	13	<0.81	14	...	3.3	5
NGC 4748 ^d	12 52 12.5	-13 24 53	63.4	Sy1	7.4	6.7	16	20	82	4
IRAS F12514+1027	12 54 00.8	+10 11 12	1667	Sy2	2.3	1.9	2.7	1.7	2.7	3
Mrk 231	12 56 14.2	+56 52 25	186	Sy1	20	<3.0	3.0	<18	<9.5	3
NGC 4826	12 56 43.7	+21 40 57	5.00	Sy2	105	<1.3	23	...	4.3	5
NGC 4818	12 56 48.9	-08 31 31	9.40	H II	185	<1.2	14	<2.0	<1.6	8
NGC 4922 ^d	13 01 24.9	+29 18 40	103	LINER	36	2.4	9.2	<1.9	4.3	2
MCG -02-33-098-E	13 02 19.7	-15 46 03	68.9	H II	32	<0.58	12	<0.61	1.2	2
MCG -02-33-098-W	13 02 20.4	-15 45 59	68.1	H II	67	<0.51	12	<0.79	<1.2	2
NGC 4941 ^{c d}	13 04 13.1	-05 33 05	15.9	Sy2	13	7.2	24	6.9	26	2
NGC 4939 ^c	13 04 14.4	-10 20 22	44.8	Sy2	8.1	12	24	17	65	2
NGC 4945 ^c	13 05 27.5	-49 28 05	8.19	Sy2	586	3.4	69	<5.1	35	2
PG 1302-102	13 05 33.0	-10 33 19	1422	QSO	0.36	0.49	0.66	0.39	2.6	1
UGC 8201	13 06 24.9	+67 42 25	3.68	<0.75	<0.24	5
NGC 4968 ^d	13 07 06.0	-23 40 37	42.6	Sy2	25	18	34	11	34	4
PG 1307+085	13 09 47.0	+08 19 48	739	QSO	0.40	0.56	0.98	0.62	0.74	1
NGC 5005 ^{c d}	13 10 56.2	+37 03 33	13.8	Sy2	37	<1.1	13	<1.2	4.6	2
PG 1309+355	13 12 17.8	+35 15 21	893	QSO	0.51	0.27	1.3	<0.30	<0.49	1
NGC 5033 ^{c d}	13 13 27.5	+36 35 38	12.4	Sy1	31	1.2	14	2.0	9.2	2
IC 860	13 15 03.5	+24 37 07	55.8	H II	3.6	<0.14	0.68	<0.48	<0.62	2
IRAS 13120-5453	13 15 06.3	-55 09 22	136	Sy2	150	1.7	18	<20	6.4	3
NGC 5055	13 15 49.3	+42 01 45	7.80	LINER	22	<0.95	9.6	...	2.3	5
UGC 8387	13 20 35.3	+34 08 22	101	H II	113	<0.54	19	<2.3	6.2	2
NGC 5104	13 21 23.1	+00 20 32	80.0	LINER	43	<0.39	5.1	<1.2	2.4	2
MCG -03-34-064 ^d	13 22 24.5	-16 43 42	71.7	Sy1	56	63	119	38	115	4
NGC 5128 ^c	13 25 27.6	-43 01 08	7.85	Sy2	197	23	150	28	135	2
NGC 5135 ^{c d}	13 25 44.1	-29 50 01	58.9	Sy2	112	14	58	18	73	2
NGC 5194 ^{c d}	13 29 52.7	+47 11 42	6.77	Sy2	44	3.0	34	3.9	19	2
NGC 5195	13 29 59.6	+47 15 58	8.00	LINER	18	<1.0	6.9	...	<1.9	5
3C 286	13 31 08.3	+30 30 32	5399	Sy1	...	0.75	0.69	6
NGC 5218	13 32 10.4	+62 46 03	41.1	H II	45	<0.16	4.9	<0.57	<2.3	2
MCG -06-30-015 ^d	13 35 53.8	-34 17 44	33.4	Sy1	5.0	5.0	5.9	7.4	26	4
IRAS F13342+3932	13 36 24.1	+39 17 31	866	Sy1	5.7	3.5	5.0	4.2	10	3
NGC 5236	13 37 00.9	-29 51 55	3.60	H II	503	<0.61	29	<1.2	5.7	7
Mrk 266 ^d	13 38 17.5	+48 16 37	116	Sy2	57	8.0	28	11	53	8
NGC 5273 ^c	13 42 08.3	+35 39 15	15.2	Sy1	2.0	<1.5	3.4	<0.88	4.9	2
Mrk 273	13 44 42.1	+55 53 12	167	LINER	42	12	34	15	56	3
IRAS F13451+1232	13 47 33.4	+12 17 24	565	Sy2	5.0	<1.0	5.1	<2.1	2.1	3
IC 4329A ^d	13 49 19.3	-30 18 34	69.6	Sy1	28	29	57	35	117	4
PG 1351+640	13 53 15.8	+63 45 45	402	QSO	1.8	<0.92	2.7	<1.00	<0.90	1
NGC 5347 ^d	13 53 17.8	+33 29 26	33.6	Sy2	4.2	2.1	4.1	<1.7	7.6	4
NGC 5371	13 55 39.9	+40 27 42	37.1	LINER	1.7	<0.090	1.1	<0.32	<0.50	2
Mrk 463	13 56 02.9	+18 22 19	222	Sy1	9.3	18	41	20	69	3
NGC 5395 ^c	13 58 38.0	+37 25 28	50.3	Sy2	...	<0.54	...	<0.31	<0.18	2
NGC 5398	14 01 21.6	-33 03 49	10.8	<0.50	<0.31	5
NGC 5408	14 03 20.9	-41 22 39	4.85	H II	...	<0.93	1.2	...	<0.51	5
NGC 5427 ^c	14 03 26.1	-06 01 50	37.5	Sy2	10	1.7	5.1	1.2	4.2	2
NGC 5474	14 05 01.6	+53 39 44	6.40	H II	...	<0.83	<0.31	5
IRAS F14070+0525	14 09 31.3	+05 11 31	1341	Sy2	1.8	<0.15	0.58	<0.60	<1.5	3
3C 295	14 11 20.6	+52 12 09	2571	Sy2	0.060	0.070	0.050	6
Circinus ^c	14 13 09.9	-65 20 20	6.09	Sy2	427	219	379	261	871	2
NGC 5506 ^{c d}	14 13 14.9	-03 12 27	26.1	Sy1	81	58	151	63	239	2
PG 1411+442	14 13 48.3	+44 00 13	411	QSO	0.36	0.96	0.92	0.55	1.5	1
NGC 5548 ^d	14 17 59.5	+25 08 12	74.5	Sy1	8.5	5.4	7.3	3.9	17	4

TABLE 1 — *Continued*

Name	R.A. ^a (J2000.0)	Decl. ^a (J2000.0)	Dist. ^b (Mpc)	Spect. Class. ^a	[Ne II] 12.81 μ m	[Ne V] 14.32 μ m	[Ne III] 15.56 μ m	[Ne V] 24.32 μ m	[O IV] 25.89 μ m	Ref.
PG 1426+015	14 29 06.6	+01 17 06	392	QSO	1.3	1.2	2.3	0.75	3.4	1
NGC 5653	14 30 10.4	+31 12 55	50.6	H II	70	<0.55	5.9	<0.25	<1.2	2
NGC 5643 ^c	14 32 40.8	-44 10 28	16.9	Sy2	38	25	56	30	121	2
Mrk 817 ^d	14 36 22.1	+58 47 39	138	Sy1	3.8	1.9	4.6	3.6	6.5	4
IRAS F14348–1447	14 37 38.4	-15 00 22	378	LINER	11	<0.21	2.6	<1.5	<3.3	3
NGC 5713	14 40 11.5	-00 17 20	29.4	H II	127	<0.80	17	...	2.8	5
IRAS F14378–3651	14 40 59.0	-37 04 32	306	LINER	11	<0.90	1.2	<2.3	<3.8	3
PG 1440+356	14 42 07.5	+35 26 22	358	QSO	4.1	1.3	3.9	1.9	6.3	1
NGC 5728 ^c	14 42 23.9	-17 15 11	40.9	Sy2	28	22	53	27	116	2
3C 303.1	14 43 14.9	+77 07 28	1358	Sy2	0.040	<0.020	0.070	...	0.090	6
NGC 5734	14 45 09.1	-20 52 13	58.0	H II	77	<0.96	8.2	<0.23	0.93	2
NGC 5743	14 45 11.0	-20 54 48	59.7	H II	50	1.3	8.9	0.78	3.2	2
PG 1448+273	14 51 08.8	+27 09 26	292	QSO	0.51	2.7	3.1	4.1	10	1
IC 4518W	14 57 41.2	-43 07 55	68.5	Sy1	40	25	49	24	85	2
IC 4518E	14 57 44.6	-43 07 53	65.4	H II	18	<0.63	1.7	<0.26	0.33	2
3C 309.1	14 59 07.6	+71 40 19	5833	Sy2	...	0.30	0.40	6
IRAS F15001+1433	15 02 31.9	+14 21 35	781	Sy2	6.8	1.1	2.6	0.66	1.7	3
PG 1501+106	15 04 01.2	+10 26 16	158	QSO	3.6	8.0	11	8.0	24	1
NGC 5866	15 06 29.5	+55 45 47	15.1	H II	7.8	<0.97	4.9	...	0.93	5
IRAS F15091–2107 ^d	15 11 59.8	-21 19 01	198	Sy1	12	8.5	16	8.1	31	4
CGCG 049-057	15 13 13.1	+07 13 31	55.8	H II	20	<0.58	1.5	<0.82	<0.59	2
NGC 5899 ^{c d}	15 15 03.2	+42 02 59	37.0	Sy2	11	6.8	16	6.7	22	2
NGC 5907	15 15 53.8	+56 19 43	12.1	H II	6.1	<0.0100	1.3	<0.070	1.6	7
VV 705	15 18 06.3	+42 44 36	178	...	62	<0.33	14	<0.79	<2.8	2
IRAS F15206+3342	15 22 38.0	+33 31 35	580	H II	13	<0.40	21	<1.5	<2.4	3
NGC 5929 ^d	15 26 06.2	+41 40 14	35.8	Sy2	13	1.1	9.8	2.2	5.3	4
IRAS 15250+3609	15 26 59.4	+35 58 37	245	LINER	10	<1.2	2.7	<2.4	<1.5	3
NGC 5936	15 30 00.8	+12 59 21	57.1	H II	82	<0.81	6.1	<0.63	1.1	2
3C 321	15 31 43.5	+24 04 19	441	Sy2	...	0.70	0.57	...	1.9	6
NGC 5953	15 34 32.4	+15 11 37	28.9	LINER	51	1.4	17	3.0	17	2
Arp 220	15 34 57.1	+23 30 11	78.2	H II	65	<2.9	7.8	<14	<21	3
IRAS 15335–0513	15 36 11.7	-05 23 52	119	H II	32	<0.19	6.1	<0.95	<1.4	2
3C 323.1	15 47 43.5	+20 52 16	1341	Sy1	0.12	<0.060	0.11	...	0.17	6
MCG -02-40-004 ^d	15 48 25.0	-13 45 27	110	Sy2	16	6.1	8.5	3.1	13	4
IRAS F15462–0450	15 48 56.8	-04 59 33	460	Sy1	7.4	<0.30	1.4	<1.0	<3.6	3
IRAS FSC15480–0344 ^d	15 50 41.5	-03 53 18	133	Sy2	5.6	6.1	9.4	8.9	35	4
3C 330	16 09 36.6	+65 56 43	3170	Sy2	...	0.40	0.40	6
IRAS F16090–0139	16 11 40.5	-01 47 05	631	LINER	7.8	<0.12	2.0	<2.0	<1.4	3
PG 1613+658	16 13 57.2	+65 43 09	605	QSO	3.9	1.1	3.3	0.65	4.9	1
IRAS 16164–0746	16 19 11.8	-07 54 02	102	LINER	47	1.2	14	<1.2	7.2	2
PG 1617+175	16 20 11.3	+17 24 27	520	QSO	0.29	<0.17	0.36	0.28	0.39	1
3C 334	16 20 21.8	+17 36 23	3212	Sy1	0.66	1.2	1.6	6
PG 1626+554	16 27 56.1	+55 22 31	626	QSO	0.069	<0.069	0.11	<0.16	<0.20	1
3C 343	16 34 33.8	+62 45 35	6510	Sy1	0.70	0.83	1.4	6
NGC 6221 ^c	16 52 46.1	-59 13 07	20.8	Sy2	196	<1.6	24	<3.1	20	2
NGC 6240	16 52 58.9	+02 24 03	105	LINER	171	4.4	61	<5.7	27	3
NGC 6285	16 58 24.0	+58 57 21	82.3	H II	18	<0.080	3.0	<0.48	1.2	2
NGC 6286	16 58 31.4	+58 56 10	79.2	LINER	29	<0.43	3.3	1.6	<0.75	2
PG 1700+518	17 01 24.8	+51 49 20	1505	QSO	1.2	<0.23	1.6	<0.43	1.7	1
3C 351	17 04 41.4	+60 44 30	1988	Sy1	0.100	0.22	0.21	6
IRAS 17138–1017	17 16 35.8	-10 20 39	74.6	H II	124	<0.81	20	<1.3	<3.4	2
NGC 6300 ^c	17 16 59.5	-62 49 14	15.9	Sy2	11	13	15	9.1	31	2
IRAS F17179+5444	17 18 54.4	+54 41 48	698	Sy2	4.5	2.2	2.9	0.82	2.1	3
IRAS 17208–0014	17 23 22.0	-00 17 00	190	H II	41	<1.00	8.1	<3.2	<2.4	3
NGC 6500	17 55 59.8	+18 20 17	43.1	LINER	4.8	<0.11	2.6	<0.49	<0.35	2
IC 4687	18 13 39.6	-57 43 31	73.8	H II	146	<0.80	45	<1.2	2.5	2
IC 4710	18 28 38.0	-66 58 56	9.00	...	0.88	<1.0	4.3	...	<0.30	5
3C 381	18 33 46.3	+47 27 02	771	Sy1	0.060	0.070	0.13	...	0.22	6
ESO 103-G035	18 38 20.3	-65 25 39	56.2	Sy2	...	18	41	6
IC 4734	18 38 25.7	-57 29 25	66.7	H II	65	<0.48	6.1	<0.66	<1.8	2
NGC 6701	18 43 12.5	+60 39 12	56.2	H II	73	<0.59	7.0	<0.63	2.1	2
NGC 6744	19 09 46.1	-63 51 27	9.90	LINER	1.1	<0.030	1.5	<0.13	<0.73	7
ESO 593-IG008	19 14 30.9	-21 19 07	218	...	32	<0.72	8.9	<0.29	<0.78	2
ESO 141-G055 ^d	19 21 14.2	-58 40 13	158	Sy1	2.2	2.2	5.6	1.6	7.3	4
IRAS F19254–7245	19 31 21.4	-72 39 18	283	Sy2	31	<2.8	13	<1.6	6.3	3
IRAS F19297–0406	19 32 21.3	-03 59 56	392	H II	18	<0.92	2.5	<2.2	<0.90	3
NGC 6814 ^c	19 42 40.6	-10 19 24	22.4	Sy1	7.2	3.2	15	6.1	27	2
NGC 6810 ^d	19 43 34.4	-58 39 20	29.2	Sy2	103	<1.1	13	<2.3	2.5	4
NGC 6860 ^d	20 08 46.9	-61 06 00	64.5	Sy1	5.6	2.8	6.7	2.4	12	4
IRAS F20087–0308	20 11 23.9	-02 59 50	490	LINER	14	<0.75	1.6	<1.9	<1.6	3
IRAS F20100–4156	20 13 29.5	-41 47 34	610	H II	7.3	<0.48	2.8	<1.3	<4.8	3
NGC 6890 ^d	20 18 18.1	-44 48 25	34.8	Sy2	11	5.8	6.6	3.8	10	4
NGC 6946	20 34 52.3	+60 09 14	6.80	H II	430	<1.5	39	...	<7.2	5
NGC 6951 ^c	20 37 14.1	+66 06 20	19.8	Sy2	40	<1.8	11	<2.0	8.2	2
Mrk 509 ^{c d}	20 44 09.7	-10 43 24	151	Sy1	11	5.1	16	7.4	28	2
IRAS F20414–1651	20 44 18.2	-16 40 16	397	LINER	6.8	1.00	1.6	<1.5	<1.8	3
IC 5063 ^d	20 52 02.3	-57 04 07	49.0	Sy2	27	30	66	24	114	4
IRAS F20551–4250	20 58 26.8	-42 39 00	190	H II	13	<0.75	2.8	<1.5	<2.0	3

TABLE 1 — *Continued*

Name	R.A. ^a (J2000.0)	Decl. ^a (J2000.0)	Dist. ^b (Mpc)	Spect. Class. ^a	[Ne II] 12.81 μ m	[Ne V] 14.32 μ m	[Ne III] 15.56 μ m	[Ne V] 24.32 μ m	[O IV] 25.89 μ m	Ref.
Mrk 897 ^d	21 07 45.8	+03 52 40	115	Sy2	24	1.1	4.4	<0.80	0.62	4
3C 433	21 23 44.5	+25 04 11	470	Sy2	1.9	2.7	5.2	...	<7.9	6
PG 2130+099	21 32 27.8	+10 08 19	283	QSO	1.4	3.7	5.7	4.0	11	1
NGC 7130 ^{c d}	21 48 19.5	-34 57 04	69.8	Sy2	82	7.1	27	4.2	15	2
NGC 7177	22 00 41.2	+17 44 17	16.1	H II	4.2	<0.11	1.5	<0.48	0.54	2
NGC 7172 ^{c d}	22 02 01.9	-31 52 11	37.2	Sy2	31	8.9	17	11	40	2
B2 2201+31A	22 03 15.0	+31 45 38	1523	QSO	0.096	0.53	0.32	<0.22	0.56	1
IRAS F22017+0319 ^d	22 04 19.2	+03 33 50	274	Sy2	5.9	8.3	14	9.4	29	4
NGC 7213 ^{c d}	22 09 16.2	-47 10 00	25.8	Sy1	24	<0.94	13	<0.73	2.4	2
IC 5179	22 16 09.1	-36 50 37	48.4	H II	113	<0.44	11	<0.81	2.0	2
PG 2214+139	22 17 12.3	+14 14 20	297	QSO	0.23	0.27	0.63	<0.31	1.3	1
NGC 7252	22 20 44.8	-24 40 41	66.4	H II	42	<0.33	3.7	<0.51	1.3	8
3C 445 ^d	22 23 49.6	-02 06 12	251	Sy1	2.3	2.0	6.2	5.8	23	4
ESO 602-G025	22 31 25.5	-19 02 04	110	LINER	44	1.6	7.6	<2.3	6.8	2
NGC 7314 ^{c d}	22 35 46.2	-26 03 00	20.6	Sy1	8.3	17	24	22	67	2
NGC 7331	22 37 04.1	+34 24 56	14.5	LINER	19	<0.52	10	...	3.0	5
MCG -03-58-007 ^d	22 49 37.1	-19 16 26	138	Sy2	8.5	6.6	9.3	3.9	8.8	4
IRAS F22491-1808	22 51 49.3	-17 52 23	354	...	5.4	<0.45	1.9	<0.90	<2.4	3
PG 2251+113	22 54 10.4	+11 36 38	1709	QSO	0.17	0.49	0.80	0.63	3.1	1
NGC 7410 ^c	22 55 00.9	-39 39 40	24.0	Sy2	3.7	<1.1	...	<1.9	<12	2
NGC 7469 ^{c d}	23 03 15.6	+08 52 26	69.8	Sy1	250	15	45	13	31	2
MCG -02-58-022	23 04 43.5	-08 41 08	213	Sy1	...	2.4	8.6	6
CGCG 453-062	23 04 56.5	+19 33 08	109	LINER	22	2.0	6.6	2.1	5.5	2
NGC 7479 ^{c d}	23 04 56.6	+12 19 22	34.2	Sy2	9.4	<2.4	5.8	<2.8	4.9	2
NGC 7496 ^{c d}	23 09 47.3	-43 25 40	22.8	Sy2	46	<0.41	6.3	<0.98	<0.48	2
IRAS F23128-5919	23 15 46.8	-59 03 15	199	Sy2	27	2.6	20	3.0	18	3
NGC 7552	23 16 10.8	-42 35 05	21.0	LINER	834	<3.6	70	...	<10	5
NGC 7591	23 18 16.3	+06 35 08	70.7	LINER	56	<0.62	5.5	<0.76	<0.54	2
NGC 7582 ^{c d}	23 18 23.5	-42 22 14	22.7	Sy2	248	36	102	60	220	2
NGC 7590 ^{c d}	23 18 54.8	-42 14 20	23.0	Sy2	6.8	<0.36	3.7	<0.52	3.0	2
IRAS F23230-6926	23 26 03.6	-69 10 18	490	LINER	7.4	<0.75	2.0	<1.2	<1.5	3
NGC 7674 ^d	23 27 56.7	+08 46 44	127	Sy2	20	21	35	17	49	4
IRAS F23253-5415	23 28 06.1	-53 58 31	610	Sy2	5.5	<0.33	1.9	1.2	1.2	3
NGC 7714	23 36 14.1	+02 09 18	38.2	LINER	103	<1.0	77	<1.8	5.5	8
IRAS F23365+3604	23 39 01.3	+36 21 08	287	LINER	8.6	<0.80	0.73	<0.54	<2.0	3
NGC 7743 ^c	23 44 21.1	+09 56 02	24.3	Sy2	4.1	<0.28	4.2	0.95	2.9	2
CGCG381-051 ^d	23 48 41.7	+02 14 23	134	Sy2	19	<0.70	1.4	<1.2	<1.3	4
NGC 7769	23 51 04.0	+20 09 01	60.2	H II	13	<0.66	3.4	<0.34	0.41	2
NGC 7771	23 51 24.9	+20 06 42	61.9	H II	108	<0.71	8.8	<0.51	1.2	2
PG 2349-014	23 51 56.1	-01 09 13	840	QSO	1.4	0.71	2.0	<0.96	3.9	1
IRAS F23498+2423	23 52 26.0	+24 40 16	1046	Sy2	3.2	1.1	2.7	2.0	5.0	3
NGC 7793	23 57 49.8	-32 35 27	3.80	H II	10	<1.0	2.6	...	<0.32	5

REFERENCES. — (1) Veilleux et al. (2009). (2) This work. (3) Farrah et al. (2007). (4) Tommasin et al. (2008, 2010). (5) Dale et al. (2009). (6) Gorjian et al. (2007). (7) Goulding & Alexander (2009). (8) Bernard-Salas et al. (2009)

NOTE. — Fluxes are expressed in units of 10^{-14} erg cm $^{-2}$ s $^{-1}$.

^a Coordinates and optical spectroscopic classification from NED.

^b We calculated the distance from the redshift assuming a flat cosmology with $H_0 = 70$ km s $^{-1}$ Mpc $^{-1}$, $\Omega_M = 0.3$, and $\Omega_\Lambda = 0.7$. Except for the galaxies from Dale et al. (2009), Bernard-Salas et al. (2009) and Goulding & Alexander (2009) for which we used the distances adopted by these authors.

^c Member of the RSA sample.

^d Member of the 12 μ m sample.

REFERENCES

- Allen, M. G., Groves, B. A., Dopita, M. A., Sutherland, R. S., & Kewley, L. J. 2008, ApJS, 178, 20
- Alonso-Herrero, A., Quillen, A. C., Rieke, G. H., Ivanov, V. D., & Efstathiou, A. 2003, AJ, 126, 81
- Alonso-Herrero, A., et al. 2009, ApJ, 697, 660
- Alonso-Herrero, A., Rieke, G. H., Rieke, M. J., Colina, L., Pérez-González, P. G., & Ryder, S. D. 2006, ApJ, 650, 835
- Antonucci, R. 1993, ARA&A, 31, 473
- Armus, L., et al. 2007, ApJ, 656, 148
- Baskin, A., & Laor, A. 2005, MNRAS, 358, 1043
- Baum, S. A., et al. 2010, ApJ, 710, 289
- Beirão, P., et al. 2008, ApJ, 676, 304
- Beirão, P., Brandl, B. R., Devost, D., Smith, J. D., Hao, L., & Houck, J. R. 2006, ApJ, 643, L1
- Bernard-Salas, J., et al. 2009, ApJS, 184, 230
- Brandl, B. R., et al. 2006, ApJ, 653, 1129
- Buchanan, C. L., Gallimore, J. F., O'Dea, C. P., Baum, S. A., Axon, D. J., Robinson, A., Elitzur, M., & Elvis, M. 2006, AJ, 132, 401
- Chapman, N. L., Mundy, L. G., Lai, S., & Evans, N. J. 2009, ApJ, 690, 496
- Chiar, J. E., & Tielens, A. G. G. M. 2006, ApJ, 637, 774
- Crenshaw, D. M., Kraemer, S. B., & George, I. M. 2003, ARA&A, 41, 117
- Crowther, P. A., Beck, S. C., Willis, A. J., Conti, P. S., Morris, P. W., & Sutherland, R. S. 1999, MNRAS, 304, 654
- Dale, D. A., et al. 2009, ApJ, 693, 1821
- Deo, R. P., Crenshaw, D. M., Kraemer, S. B., Dietrich, M., Elitzur, M., Teplitz, H., & Turner, T. J. 2007, ApJ, 671, 124
- Diamond-Stanic, A. M., & Rieke. 2010, ApJ, submitted
- Diamond-Stanic, A. M., Rieke, G. H., & Rigby, J. R. 2009, ApJ, 698, 623

- Díaz-Santos, T., Alonso-Herrero, A., Colina, L., Packham, C., Levenson, N. A., Pereira-Santaella, M., Roche, P. F., & Telesco, C. M. 2010, ApJ, 711, 328
- Dudik, R. P., Satyapal, S., & Marcu, D. 2009, ApJ, 691, 1501
- Dudik, R. P., Weingartner, J. C., Satyapal, S., Fischer, J., Dudley, C. C., & O'Halloran, B. 2007, ApJ, 664, 71
- Farrah, D., et al. 2007, ApJ, 667, 149
- Flaherty, K. M., Pipher, J. L., Megeath, S. T., Winston, E. M., Gutermuth, R. A., Muzeirole, J., Allen, L. E., & Fazio, G. G. 2007, ApJ, 663, 1069
- Genzel, R., et al. 1998, ApJ, 498, 579
- Gorjian, V., Cleary, K., Werner, M. W., & Lawrence, C. R. 2007, ApJ, 655, L73
- Goulding, A. D., & Alexander, D. M. 2009, MNRAS, 398, 1165
- Groves, B., Dopita, M., & Sutherland, R. 2006, A&A, 458, 405
- Groves, B. A., Dopita, M. A., & Sutherland, R. S. 2004, ApJS, 153, 9
- Ho, L. C., Filippenko, A. V., & Sargent, W. L. W. 1997, ApJS, 112, 315
- Ho, L. C., & Keto, E. 2007, ApJ, 658, 314
- Houck, J. R., et al. 2004, ApJS, 154, 18
- Imanishi, M., & Wada, K. 2004, ApJ, 617, 214
- Jiang, B. W., Gao, J., Omont, A., Schuller, F., & Simon, G. 2006, A&A, 446, 551
- Kauffmann, G., et al. 2003, MNRAS, 346, 1055
- Kraemer, S. B., Turner, T. J., Crenshaw, D. M., & George, I. M. 1999, ApJ, 519, 69
- Lutz, D., Kunze, D., Spoon, H. W. W., & Thornley, M. D. 1998a, A&A, 333, L75
- Lutz, D., Spoon, H. W. W., Rigopoulou, D., Moorwood, A. F. M., & Genzel, R. 1998b, ApJ, 505, L103
- Maiolino, R., & Rieke, G. H. 1995, ApJ, 454, 95
- Maiolino, R., Ruiz, M., Rieke, G. H., & Keller, L. D. 1995, ApJ, 446, 561
- McClure, M. 2009, ApJ, 693, L81
- Meléndez, M., et al. 2008a, ApJ, 682, 94
- Meléndez, M., Kraemer, S. B., Schmitt, H. R., Crenshaw, D. M., Deo, R. P., Mushotzky, R. F., & Bruhwiler, F. C. 2008b, ApJ, 689, 95
- Nagao, T., Murayama, T., & Taniguchi, Y. 2001, ApJ, 546, 744
- Ochsenbein, F., Bauer, P., & Marcout, J. 2000, A&AS, 143, 23
- Ogle, P., Whysong, D., & Antonucci, R. 2006, ApJ, 647, 161
- Oliva, E., Moorwood, A. F. M., Drapatz, S., Lutz, D., & Sturm, E. 1999, A&A, 343, 943
- Osterbrock, D. E., & Ferland, G. J. 2006, Astrophysics of gaseous nebulae and active galactic nuclei, ed. D. E. Osterbrock & G. J. Ferland
- Peeters, E., Spoon, H. W. W., & Tielens, A. G. G. M. 2004, ApJ, 613, 986
- Pereira-Santaella, M., Alonso-Herrero, A., Rieke, G. H., Colina, L., Díaz-Santos, T., Smith, J.-D. T., Pérez-González, P. G., & Engelbracht, C. W. 2010, ApJS accepted (arXiv:1004.1364)
- Pottasch, S. R., Surendiranath, R., Bernard-Salas, J., & Roellig, T. L. 2009, A&A, 502, 189
- Ramos Almeida, C., et al. 2009, ApJ, 702, 1127
- Rigby, J. R., Diamond-Stanic, A. M., & Aniano, G. 2009, ApJ, 700, 1878
- Rigby, J. R., & Rieke, G. H. 2004, ApJ, 606, 237
- Roche, P. F., Aitken, D. K., Smith, C. H., & Ward, M. J. 1991, MNRAS, 248, 606
- Rosenthal, D., Bertoldi, F., & Drapatz, S. 2000, A&A, 356, 705
- Rush, B., Malkan, M. A., & Spinoglio, L. 1993, ApJS, 89, 1
- Sanders, D. B., Mazzarella, J. M., Kim, D.-C., Surace, J. A., & Soifer, B. T. 2003, AJ, 126, 1607
- Sanders, D. B., & Mirabel, I. F. 1996, ARA&A, 34, 749
- Satyapal, S., Sambruna, R. M., & Dudik, R. P. 2004, A&A, 414, 825
- Satyapal, S., Vega, D., Dudik, R. P., Abel, N. P., & Heckman, T. 2008, ApJ, 677, 926
- Schaerer, D., & Stasińska, G. 1999, A&A, 345, L17
- Shi, Y., Rieke, G. H., Ogle, P., Jiang, L., & Diamond-Stanic, A. M. 2009, ApJ, 703, 1107
- Smith, J. D. T., Rudnick, L., Delaney, T., Rho, J., Gomez, H., Kozasa, T., Reach, W., & Isensee, K. 2009, ApJ, 693, 713
- Snijders, L., Kewley, L. J., & van der Werf, P. P. 2007, ApJ, 669, 269
- Sturm, E., Lutz, D., Verma, A., Netzer, H., Sternberg, A., Moorwood, A. F. M., Oliva, E., & Genzel, R. 2002, A&A, 393, 821
- Sturm, E., et al. 2006, ApJ, 653, L13
- Surace, J. A., Sanders, D. B., & Mazzarella, J. M. 2004, AJ, 127, 3235
- Takeuchi, T. T., Yoshikawa, K., & Ishii, T. T. 2003, ApJ, 587, L89
- Thornley, M. D., Schreiber, N. M. F., Lutz, D., Genzel, R., Spoon, H. W. W., Kunze, D., & Sternberg, A. 2000, ApJ, 539, 641
- Tommasin, S., Spinoglio, L., Malkan, M. A., & Fazio, G. 2010, ApJ, 709, 1257
- Tommasin, S., Spinoglio, L., Malkan, M. A., Smith, H., González-Alfonso, E., & Charmandaris, V. 2008, ApJ, 676, 836
- Urry, C. M., & Padovani, P. 1995, PASP, 107, 803
- Veilleux, S., et al. 2009, ApJS, 182, 628
- Verma, A., Lutz, D., Sturm, E., Sternberg, A., Genzel, R., & Vacca, W. 2003, A&A, 403, 829
- Weaver, K. A., et al. 2010, arXiv:1004.5321
- Weedman, D. W., et al. 2005, ApJ, 633, 706